Toward the RNA-World in the Interstellar Medium—Detection of Urea and Search of 2-Amino-oxazole and Simple Sugars

Izaskun Jiménez-Serra,[1] Jesús Martín-Pintado,[1] Víctor M. Rivilla,[2] Lucas Rodríguez-Almeida,[1] Elena R. Alonso Alonso,[3,4] Shaoshan Zeng,[5] Emilio J. Cocinero,[3,4] Sergio Martín,[6,7] Miguel Requena-Torres,[8] Rafa Martín-Domenech,[9] and Leonardo Testi[10,2]

Abstract

In the past decade, astrochemistry has witnessed an impressive increase in the number of detections of complex organic molecules. Some of these species are of prebiotic interest such as glycolaldehyde, the simplest sugar, or aminoacetonitrile, a possible precursor of glycine. Recently, we have reported the detection of two new nitrogen-bearing complex organics, glycolonitrile and Z-cyanomethanimine, known to be intermediate species in the formation process of ribonucleotides within theories of a primordial RNA-world for the origin of life. In this study, we present deep and high-sensitivity observations toward two of the most chemically rich sources in the galaxy: a giant molecular cloud in the center of the Milky Way **(G + 0.693-0.027)** and a proto-Sun **(IRAS16293-2422 B)**. Our aim is to explore whether the key precursors considered to drive the primordial RNA-world chemistry are also found in space. Our high-sensitivity observations reveal that urea is present in G + 0.693-0.027 with an abundance of $\sim 5 \times 10^{-11}$. This is the first detection of this prebiotic species outside a star-forming region. Urea remains undetected toward the proto-Sun IRAS16293-2422 B (upper limit to its abundance of $\leq 2 \times 10^{-11}$). Other precursors of the RNA-world chemical scheme such as glycolaldehyde or cyanamide are abundant in space, but key prebiotic species such as 2-amino-oxazole, glyceraldehyde, or dihydroxyacetone are not detected in either source. Future more sensitive observations targeting the brightest transitions of these species will be needed to disentangle whether these large prebiotic organics are certainly present in space. Key Words: Astrochemistry—Radioastronomy—Molecules—Prebiotic chemistry. Astrobiology 20, 1048–1066.

1. Introduction

THE QUESTION OF THE ORIGIN of life has intrigued human beings for centuries. Life appeared on Earth about 4 billion years ago, but we do not know the processes that made it possible. One of the proposed scenarios is the so-called RNA-world, which suggests that early forms of life relied solely on (RNA) to store genetic information and to catalyze chemical reactions.

The RNA-world hypothesis was originally not very popular among the astrobiology community because it was far from trivial to form RNA from its main constituents: a nitrogenous base, a ribose sugar, and a phosphate. Even the prebiotic formation of these basic building blocks of the RNA is still, so far, unknown. In recent years, however, it has become clear that ribonucleotides could have formed, instead, from simpler molecules such as cyanamide (NH_2CN), cyanoacetylene, or glycolaldehyde [$CH_2(OH)CHO$], all

[1]Departamento de Astrofísica, Centro de Astrobiología (INTA-CSIC), Madrid, Spain.
[2]INAF-Osservatorio Astrofisico di Arcetri, Florence, Italy.
[3]Departamento de Química Física, Facultad de Ciencia y Tecnología, Universidad del País Vasco, (UPV-EHU), Bilbao, Spain.
[4]Biofisika Institute (CSIC, UPV/EHU), Leioa, Spain.
[5]School of Physics and Astronomy, Queen Mary University of London, London, United Kingdom.
[6]European Southern Observatory, Vitacura, Chile.
[7]Joint ALMA Observatory, Vitacura, Chile.
[8]Department of Astronomy, University of Maryland, College Park, Maryland.
[9]Harvard-Smithsonian Center for Astrophysics, Cambridge, Massachusetts.
[10]European Southern Observatory, Garching bei München, Germany.

derivatives of hydrogen cyanide (HCN) in an aqueous medium (Powner *et al.*, 2009; Patel *et al.*, 2015).

Astrochemistry is the discipline that studies the chemical processes taking place in space. Since the detection of the first molecular ions and radicals in space in the 1930s and 1940s (*e.g.*, CN, CH, and CH$^+$; Swings and Rosenfeld, 1937; Douglas and Herzberg, 1941), astrochemistry has witnessed an impressive increase in the number of molecular species detected in the gas phase in both the circumstellar medium (CSM; in particular around evolved stars) and in the interstellar medium (ISM, especially in regions forming stars). The average detection rate of new molecules in the CSM/ISM is currently about 4 species per year, and over 200 gas-phase molecular species are known to be present in space (see figure 1 in McGuire, 2018).

Among the detected molecules, complex organic molecules (or COMs, defined as carbon-bearing compounds with six atoms or more in their molecular structure; Herbst and van Dishoeck, 2009) have attracted much interest in recent years due to their link to prebiotic chemistry. Molecular searches in the ISM have indeed been very prolific in the detection of molecules of prebiotic relevance with relatively high abundances such as NH$_2$CN (Turner *et al.*, 1975), CH$_2$(OH)CHO (Hollis *et al.*, 2000), or even urea (NH$_2$CONH$_2$; Belloche *et al.*, 2019), which hints to a high level of chemical complexity in space. The question that follows is: Should one expect to find in the ISM the same chemical precursors as those of the RNA-world hypothesis for the origin of life?

Recently, we have reported the first detection of glycolonitrile (HOCH$_2$CN) in space (or hydroxyacetonitrile, HOCH$_2$CN; Zeng *et al.*, 2018). In the RNA-world scenario, HOCH$_2$CN is an intermediate species in the reductive homologation of HCN, and it is key in the construction of sugars [*e.g.*, CH$_2$(OH)CHO and glyceraldehyde (CHO-CHOHCH$_2$OH)] needed for ribonucleotide assembly (Patel *et al.*, 2015).

The advent of a wide-band, very sensitive instrumentation in radiotelescopes such as the broad-band Eight MIxer Receivers (EMIRs) at the Instituto de Radioastronomía Milimétrica (IRAM) 30-m-diameter telescope or the Atacama Large Millimeter/Sub-millimeter Array (ALMA), together with the high degree of chemical complexity observed in the ISM, offers a unique opportunity to investigate to what extent the RNA-world chemical scheme proposed in the works of Powner *et al.* (2009) and Patel *et al.* (2015) for the origin of life can be extrapolated to the ISM.

In this study, we explore whether precursors of pyrimidine ribonucleotides (according to the RNA-world chemical scheme of Powner *et al.*, 2009 and Patel *et al.*, 2015) are found in the ISM and star forming regions in our galaxy. To do this, we use high-sensitivity spectral surveys carried out toward a proto-Sun and a quiescent giant molecular cloud (GMC) in the Galactic Center to detect and determine the molecular abundances of species such as CHOCHOH-CH$_2$OH, dihydroxyacetone (DHA—CH$_2$OHCOCH$_2$OH), and 2-amino-oxazole (C$_3$H$_4$N$_2$O), key precursors in the primordial RNA-world chemical scheme. These molecules remain undiscovered in space so far. To our knowledge, this is the first attempt to find C$_3$H$_4$N$_2$O in the ISM, a central molecule in the scheme proposed in the works of Powner *et al.* (2009) and Patel *et al.* (2015).

Our high-sensitivity observations reveal that NH$_2$CONH$_2$ is a natural product of COM interstellar chemistry even without the intervention of star formation. Other key species in the primordial RNA-world chemical scheme such as C$_3$H$_4$N$_2$O or DHA are not detected in our deep integrations, with upper limits to their abundance relative to molecular hydrogen of a few $\leq 10^{-11} - 10^{-10}$. The detection of these large COM precursors in the ISM would allow the field of *Astrochemistry to transition to Astrobiochemistry, that is, to the study of biologically relevant prebiotic compounds in space.*

2. Materials and Methods

2.1. Targeted molecular species

In Fig. 1, we show a summary of the chemical scheme proposed for the synthesis of (pyrimidine) ribonucleotides, nucleobases (cytosine), and amino acids (glycine or NH$_2$CH$_2$COOH) within the RNA-world hypothesis for the origin of life (Powner *et al.*, 2009; Patel *et al.*, 2015; Kitadai and Maruyama, 2018). Another gas-phase route recently proposed by Rivilla *et al.* (2019b) for the formation of adenine in space has also been added to this diagram. Molecules detected already in the ISM and star-forming regions are indicated with solid-line boxes, while (so far) undetected molecules are shown within dotted-line boxes.

The goal of this diagram is to visualize at once how many RNA-world prebiotic species have been detected in the ISM, and how they are related to each other according to the works of Powner *et al.* (2009), Patel *et al.* (2015), Kitadai and Maruyama, (2018), and Rivilla *et al.* (2019b). This diagram is not meant to imply any specific chemical reaction occurring in the ISM (because most of them take place in aqueous solution), but to identify the prebiotic species that are central in the primordial RNA-world theory for the origin of life, and that could be observed with current and future astronomical instrumentation.

The molecular species for which spectroscopic information is available from either the Cologne Database for Molecular Spectroscopy (CDMS; Endres *et al.*, 2016)[†] or from the Jet Propulsion Laboratory (JPL) catalog (Pickett *et al.*, 1998)[‡] are (Tables 1 and 2) as follows: HCN, formaldehyde (H$_2$CO), HOCH$_2$CN, CH$_2$(OH)CHO, NH$_2$CN, glycolic acid (CH$_2$OHCOOH), methanimine (CH$_2$NH), NH$_2$CONH$_2$, cyanomethanimine (E/Z-HNCHCN), aminoacetonitrile (NH$_2$CH$_2$CN), CHOCHOHCH$_2$OH, DHA—CH$_2$OHCOCH$_2$OH, and NH$_2$CH$_2$COOH.

The microwave spectrum of the 0$^+$ and 0$^-$ states of C$_3$H$_4$N$_2$O (currently unavailable in molecular spectroscopy databases) was recorded and analyzed by Møllendal and Konovalov (2010). These authors obtained the microwave spectrum of C$_3$H$_4$N$_2$O between 26.6 and 80 GHz by means of Stark-modulation spectroscopy. Due to the inversion of the amino group, there is a double-minimum potential that is manifested with the splitting of the lines into closely spaced doublets of comparable intensities, leading to two states designated as 0$^+$ and 0$^-$. From the fitting of the measured transitions with the Pickett's Spectral Fitting/Spectral

---

[†]http://www.astro.uni-koeln.de/cdms
[‡]https://spec.jpl.nasa.gov
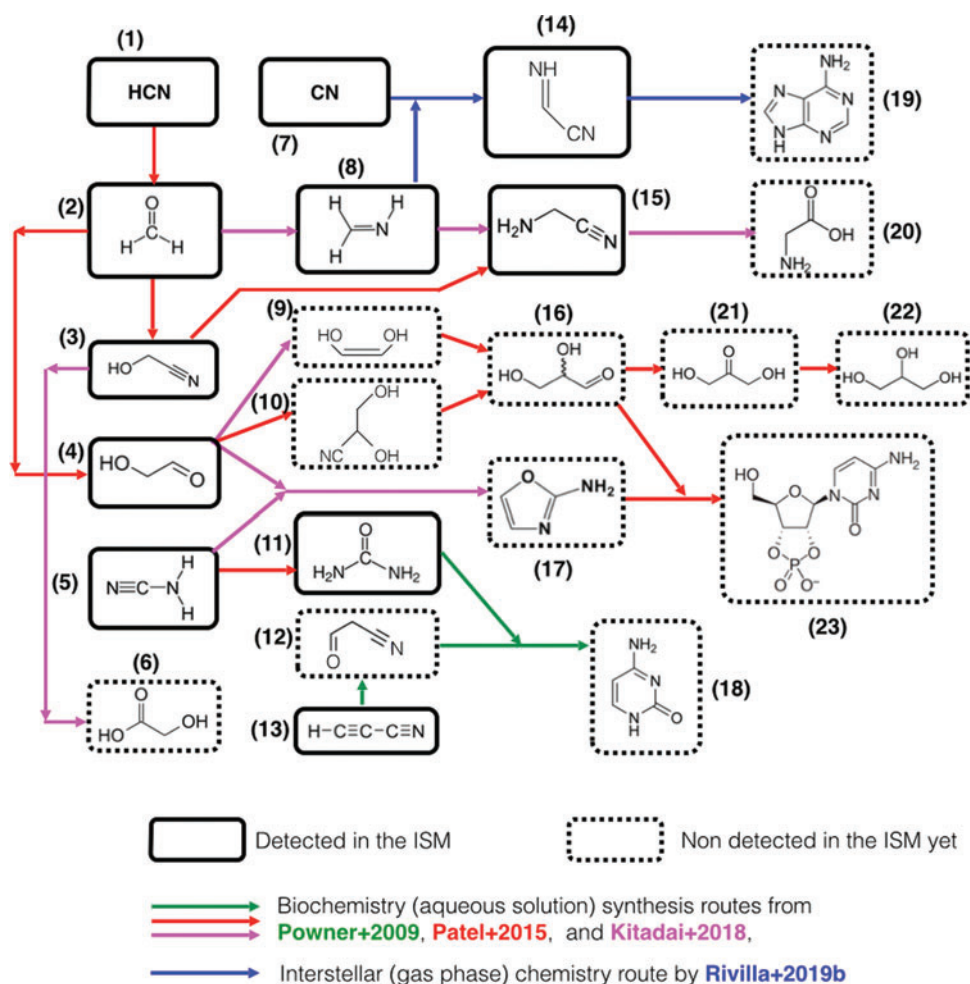
FIG. 1. Summary of the chemical scheme of the RNA-world scenario. Extracted from Powner *et al.* (2009), Patel *et al.* (2015), Kitadai and Maruyama (2018), and Rivilla *et al.* (2019b; see the different colors for the arrows). Solid-line boxes indicate molecules that have been detected in space, while dotted-line boxes denote those species that remain undetected in space. The goal of this diagram is to visualize at once how many primordial RNA-world prebiotic species have been detected in the ISM, and how they are related to each other. The names of the molecules shown are as follows: (1) hydrogen cyanide; (2) formaldehyde; (3) glycolonitrile; (4) glycolaldehyde; (5) cyanamide; (6) glycolic acid; (7) cyanide; (8) methenamine; (9) enol form of glycolaldehyde; (10) cyanohydrin; (11) urea; (12) 3-oxopropanenitrile; (13) cyanoacetylene; (14) cyanomethanimine; (15) aminoacetonitrile; (16) glyceraldehyde; (17) 2-amino-oxazole; (18) cytosine; (19) adenine; (20) glycine; (21) dihydroxyacetone (DHA); (22) glycerol; (23) beta-ribocytidine-2′,3′-cyclic phosphate (pyrimidine ribonucleotide). HCN, hydrogen cyanide; ISM, interstellar medium. Color images are available online.

Catalogue program suite (Pickett, 1991), two sets of experimental rotational parameters, including quartic centrifugal distortion constants, were obtained for the 0^+ and 0^- states. The spectroscopic information of these two states can be found in Table 3. For the details about the spectroscopic work of Møllendal and Konovalov (2010), please refer to their article.

Due to the lack of an entry for $C_3H_4N_2O$ in molecular line catalogs such as JPL and CDMS, we have generated two transition files (*.cat files in Supplementary Data) for the 0^+ and 0^- states of $C_3H_4N_2O$, which have been implemented into the millimeter/submillimeter data analysis software Madrid Data Cube Analysis (MADCUBA) (Section 3.1). In this study, we use these data to search for $C_3H_4N_2O$ toward two astronomical sources, a proto-Sun and a GMC located in the central region of the Milky Way.

2.2. Astronomical sources

Our selected astronomical sources are the solar-type protostar IRAS16293-2422 B and the quiescent GMC G+0.693-0.027 located in the galactic center. These two sources are among the richest ISM regions in COMs within our galaxy, making them excellent targets for the search of new molecules in space (Requena-Torres *et al.*, 2008; Jørgensen *et al.*, 2016; Martín-Doménech *et al.*, 2017; Zeng *et al.*, 2018, 2019).

They are located in two completely different environments: while IRAS16293-2422 B is part of a typical low-mass star-forming region in the galactic disk just affected by the standard ultraviolet (UV) interstellar radiation field and standard cosmic-ray ionization rate (*i.e.*, $G_0 = 1$ Habing or 1.6×10^{-3} ergs (cm^{-2}·s^{-1}) $\xi = 3 \times 10^{-17}$ s^{-1}), G+0.693-0.027 is exposed to multiple highly energetic phenomena taking

TABLE 1. PHYSICAL PARAMETERS DERIVED FOR THE PREBIOTIC MOLECULES FROM THE RNA-WORLD CHEMICAL SCHEME OBSERVED TOWARD THE HOT CORINO IRAS16293-2422 B

Molecule name	Formula	T_{ex} (K)	V_{LSR} (km/s)	Δv (km/s)	N (cm^{-2})	χ^d	Reference
Hydrogen cyanide (^{15}N)	HC^{15}N	150^a	2.42±0.03	1.29±0.05	≥3.5×10^{14,e}	≥1.3×10^{-11}	This work; see also Takakuwa *et al.* (2007)
Formaldehyde (^{18}O)	H$_2$C^{18}O	99±11	2.65±0.02	0.98±0.06	(3.5±0.3)×10^{15}	1.3×10^{-10}	This work; see also Persson *et al.* (2018)
Glycolonitrile (hot)	HOCH$_2$CN	158±38	2.62±0.15	1.03±0.03^b	(1.8±0.1)×10^{15,b}	6.5×10^{-11}	Zeng *et al.* (2019)
Glycolaldehyde	CH$_2$(OH)CHO	284–300	...	...	(3.3–6.8)×10^{16}	(1.2–2.4)×10^{-9}	From Jørgensen *et al.* (2016); Rivilla *et al.* (2019a)
Cyanamide (hot)	NH$_2$CN	290±40	2.76±0.04	1.03^{b,c}	(5.2±0.6)×10^{14,b}	1.9×10^{-11}	This work; see also Coutens *et al.* (2018)
Methanimine	CH$_2$NH	150^a	3.3±0.3	2.0±0.9	(4.0±0.8)×10^{15}	1.4×10^{-10}	This work; see also Ligterink *et al.* (2018)
Glycolic acid	CH$_2$OHCOOH	150^a	...	...	≤1.2×10^{14}	≤4.3×10^{-12}	This work
Urea	NH$_2$CONH$_2$	150^a	...	...	≤6.5×10^{14}	≤2.3×10^{-11}	This work
E-cyanomethanimine	E-HNCHCN	150^a	...	...	≤8.7×10^{13}	≤3.1×10^{-12}	This work
Z-cyanomethanimine	Z-HNCHCN	150^a	...	...	≤1.0×10^{15}	≤3.6×10^{-11}	This work
Aminoacetonitrile	NH$_2$CH$_2$CN	150^a	...	...	≤1.2×10^{14}	≤4.3×10^{-12}	This work
Glyceraldehyde	CHOCHOHCH$_2$OH	150^a	...	...	≤1.6×10^{15}	≤5.7×10^{-11}	This work
Dihydroxyacetone (DHA)	CH$_2$OHCOCH$_2$OH	150^a	...	...	≤1.1×10^{16}	≤3.9×10^{-10}	This work
Glycine (conformer I)	NH$_2$CH$_2$COOH	150^a	...	...	≤5.8×10^{15}	≤2.1×10^{-10}	This work
2-Amino-oxazole 0$^+$	C$_3$H$_4$N$_2$O 0$^+$	150^a	...	...	≤3.2×10^{14}	≤1.1×10^{-11}	This work
2-Amino-oxazole 0$^-$	C$_3$H$_4$N$_2$O 0$^-$	150^a	...	...	≤1.1×10^{15}	≤3.9×10^{-11}	This work

The lines from all these COMs toward IRAS16293-2422 were identified in the data and synthetic spectra were generated and fitted with the MADCUBA software to constrain the N_{tot}, T_{ex}, V_{LSR}, and Δv of the emission.

^{a}T$_{ex}$ fixed to this value within the MADCUBA-AUTOFIT analysis tool.

^{b}Molecule required two temperature components to fit the observed spectra.

^{c}Δv had to be fixed for the MADCUBA-AUTOFIT tool to converge.

^{d}Molecular abundances with respect to H$_2$ calculated assuming N(H$_2$)=2.8×10^{25} cm^{-2} (Martín-Doménech *et al.*, 2017).

^{e}The HC^{15}N line is optically thick (optical depth of 1.4) and thus its derived column density is a lower limit.

Δv, linewidth; AUTOFIT, automatic fitting tool within MADCUBA; COMs, complex organic molecules; MADCUBA, Madrid Data Cube Analysis; N$_{tot}$, molecular column density; T$_{ex}$, excitation temperature; V$_{LSR}$, central radial velocity.

TABLE 2. PHYSICAL PARAMETERS DERIVED FOR THE PREBIOTIC MOLECULES FROM THE RNA-WORLD CHEMICAL SCHEME
OBSERVED TOWARD THE QUIESCENT GIANT MOLECULAR CLOUD G+0.693-0.027

Molecule name	Formula	T_{ex} (K)	V_{LSR} (km/s)	Δv (km/s)	N (cm^{-2})	χ[f]	Reference
Hydrogen cyanide (^{15}N)	HC^{15}N	4.7 ± 0.3	71.6 ± 0.5	22 ± 1	$(1.1 \pm 0.1) \times 10^{13}$	3.0×10^{-10}	From Zeng et al. (2018)
Formaldehyde (^{13}C)	H$_2^{13}$CO	6.6 ± 0.1	70.4 ± 0.1	19.8 ± 0.2	$(2.00 \pm 0.03) \times 10^{13}$	1.5×10^{-10}	This study
Glycolonitrile	HOCH$_2$CN	8[c]	...	20[d]	$\leq 7.7 \times 10^{12}$	$\leq 5.7 \times 10^{-11}$	This study
Glycolaldehyde	CH$_2$(OH)CHO	8[c]	70[d]	20[d]	$(3.31 \pm 0.04) \times 10^{13}$	2.5×10^{-10}	This study
Cyanamide	NH$_2$CN	6.6[a]	67[a]	24[a]	$(3.1 \pm 0.2) \times 10^{14,b}$	2.3×10^{-9}	From Zeng et al. (2018)
Methanimine	CH$_2$NH	9.7 ± 0.4	69 ± 1	25 ± 1	$(5.4 \pm 0.3) \times 10^{14}$	4.3×10^{-9}	From Zeng et al. (2018)
Glycolic acid	CH$_2$OHCOOH	8[c]	...	20[d]	$\leq 2.3 \times 10^{13}$	$\leq 1.7 \times 10^{-10}$	This study
Urea	NH$_2$CONH$_2$	8[c]	...	20[d]	$(6.3 \pm 0.1) \times 10^{12}$	4.7×10^{-11}	This study
E-cyanomethanimine	E-HNCHCN	8[c]	68.0 ± 0.8	21 ± 2	$(0.33 \pm 0.03) \times 10^{14}$	2.4×10^{-10}	From Rivilla et al. (2019b)
Z-cyanomethanimine	Z-HNCHCN	8 ± 2	68.3 ± 0.8	20[d]	$(2.0 \pm 0.6) \times 10^{14}$	1.5×10^{-9}	From Rivilla et al. (2019b)
Aminoacetonitrile	NH$_2$CH$_2$CN	15[e]	...	20[d]	$\leq 0.6 \times 10^{13}$	$\leq 4.7 \times 10^{-11}$	From Zeng et al. (2018)
Glyceraldehyde	CHOCHOHCH$_2$OH	8[c]	...	20[d]	$\leq 1.3 \times 10^{13}$	$\leq 9.3 \times 10^{-11}$	This study
Dihydroxyacetone (DHA)	CH$_2$OHCOCH$_2$OH	8[c]	...	20[d]	$\leq 6.8 \times 10^{12}$	$\leq 5.0 \times 10^{-11}$	This study
Glycine (conformer I)	NH$_2$CH$_2$COOH	8[c]	...	20[d]	$\leq 5.6 \times 10^{13}$	$\leq 4.1 \times 10^{-10}$	This study
2-Amino-oxazole 0^+	C$_3$H$_4$N$_2$O 0^+	8[c]	...	20[d]	$\leq 1.1 \times 10^{13}$	$\leq 8.1 \times 10^{-11}$	This study
2-Amino-oxazole 0^-	C$_3$H$_4$N$_2$O 0^-	8[c]	...	20[d]	$\leq 1.1 \times 10^{13}$	$\leq 8.1 \times 10^{-11}$	This study

The same analysis procedure was followed as for Table 1 with the MADCUBA software developed at the Center for Astrobiology in Madrid.

[a]Average values between the ortho and para forms of NH$_2$CN (see also Zeng et al., 2018).
[b]Total column density calculated adding the column densities derived from the ortho and para forms of NH$_2$CN.
[c]Temperature fixed to the T_{ex} inferred for Z-HNCHCN, so that the MADCUBA-AUTOFIT tool could converge.
[d]Δv and V_{LSR} fixed to the typical value of the molecular emission in G+0.693-0.027 so that MADCUBA-AUTOFIT could converge.
[e]As assumed in Zeng et al. (2018).
[f]Molecular abundances with respect to H$_2$ calculated assuming N(H$_2$) = 1.35×10^{23} cm^{-2} (Martín et al., 2008).

place in the galactic center such as shock waves and enhanced cosmic rays. This will allow us to explore the effects of energy injection into the production of prebiotic COMs in the ISM. In fact, the chemistry of COMs in the quiescent GMC G+0.693-0.027 can be used as a proxy of the COM chemistry experienced by the molecular cloud from which the protosolar nebula emerged, since the latter likely underwent energetic processing by shock waves and enhanced cosmic rays as a result of (at least) one supernova explosion.[§]

IRAS16293-2422 B is a prototypical low-mass protostar that belongs to a multiple system in the ρ Ophiuchi star-forming cluster at a distance of ∼141 pc (Dzib et al., 2018). With a luminosity of ≤3 Lo, this source represents the early stages in the formation of a solar-type system (i.e., a proto-Sun). IRAS16293-2422 B is surrounded by a *hot corino*, a very dense (>10^7 cm^{-3}; Jørgensen et al., 2016; Hernández-Gómez et al., 2019), warm (>100 K; Ceccarelli et al., 2000; Bisschop et al., 2008), and compact condensation (∼100 au; Zapata et al., 2013), which surrounds the nascent solar-type protostar and where planets are expected to form. As a

result of the high temperatures, the ice mantles from dust grains are sublimated, releasing all their organic content into the gas phase of the ISM. A wide variety of COMs have been reported toward this source (Caux et al., 2011; Jaber et al., 2014; Jørgensen et al., 2016; Rivilla et al., 2019a).

G+0.693-0.027 is a massive GMC about 2.4 pc wide assuming a distance to the galactic center of 8.34 kpc (Reid et al., 2014) located within the central molecular zone (i.e., the central 500 pc) of the Milky Way (Morris and Serabyn, 1996). Because of its location in the galactic center, the molecular gas in G+0.693-0.027 is affected by highly energetic phenomena such as low-velocity shocks and/or enhanced cosmic-ray ionization rates (Requena-Torres et al., 2006; Martín et al., 2008; Zeng et al., 2018). As a result, the physical conditions of G+0.693-0.027 are very different from those of IRAS16293-2422 B.

Like the hot corino, G+0.693-0.027 presents high gas kinetic temperatures (between ∼50 and ∼140 K; Guesten et al., 1985; Hüettemeister et al., 1993; Krieger et al., 2017; Zeng et al., 2018). However, while in the hot corino, gas and dust are thermally coupled due to the high densities of the gas (>10^7 cm^{-3}), the H$_2$ gas density in G+0.693-0.027 is low (∼10^4 cm^{-3}), which yields also low dust temperatures (≤30 K; Rodríguez-Fernández et al., 2000, 2004). In addition, G+0.693-0.027 does not show any sign of star formation activity (in the form of water masers, infrared (IR) or

[§]The detection of short-lived radioactive species in meteorites suggests that the Sun's birthplace may have been a massive cluster affected by at least one supernova event (Adams, 2010).

TABLE 3. EXPERIMENTAL SPECTROSCOPIC CONSTANTS
OF THE GROUND VIBRATIONAL STATES
OF 2-AMINO-OXAZOLE USED TO CREATE *.CAT FILE

	0^+	0^-
A/MHz	9326.4892 (16)[a]	9323.9447 (18)
B/MHz	3912.38508 (65)	3907.47653 (72)
C/MHz	2760.84451 (64)	2760.31584 (65)
Δ_J/kHz	0.29626 (50)	0.29703 (52)
Δ_{JK}/kHz	1.1527 (55)	1.1568 (59)
Δ_K/kHz	1.7972 (26)	1.7881 (27)
δ_J/kHz	0.08323 (45)	0.08220 (41)
δ_K/kHz	1.1305 (97)	1.141 (10)
N_{lines}	527	458

Spectroscopic constants of the ground vibrational states of $C_3H_4N_2O$. These constants have been extracted from the experimental work of Møllendal and Konovalov (2010), and they have been used to create the *.cat files provided in the Supplementary Data. These files include the information of the rotational transitions of the 0^+ and 0^- states of $C_3H_4N_2O$ with their frequencies, energies of the lower level (E_l), intensities at 300 K (in logarithmic scale), and quantum numbers.

[a]The numbers in parentheses are 1σ uncertainties in units of the last decimal digit.

millimeter (mm) continuum sources, or ultracompact HII regions (Ginsburg *et al.*, 2018).

As found by Requena-Torres *et al.* (2008), G + 0.693-0.027 is the quiescent GMC in the galactic center with the highest level of chemical complexity, similar to that found in typical massive hot molecular cores such as SgrB2(N) (Belloche *et al.*, 2013). Large COMs such as propenal and propanal have been reported toward this cloud (Requena-Torres *et al.*, 2008), as well as many N-bearing COMs, including CH_2NH, methyl isocyanate (CH_3NCO), formamide (NH_2CHO) or cyanomethanimine (HNCHCN; Zeng *et al.*, 2018; Rivilla *et al.*, 2019b). G + 0.693-0.027 is also the only GMC in the galactic center where the prebiotic molecule phosphorus monoxide (PO) has been found (Rivilla *et al.*, 2018). All this makes G + 0.693-0.027 not only the largest COM reservoir in our galaxy (Requena-Torres *et al.*, 2008), but also an excellent laboratory where to find prebiotic precursors of the RNA-world.

We note that data from other hot molecular cores such as SgrB2 (N), Orion KL, W51, or NGC6334 I do exist in the ALMA data archive. However, the spectral surveys presented in this work likely suffer less from line confusion because: (1) the molecular emission toward IRAS16293-2422 B, as observed with ALMA, has linewidths significantly narrower than those measured toward the aforementioned hot cores; and (2) the COM emission in the quiescent GMC G + 0.693-0.027 is subthermally excited (derived excitation temperatures [T_{ex}] < 15 K; Section 3.1), which implies that only the lowest energy levels of the observed COMs are populated reducing the level of line confusion.

2.3. Observations

Due to the different spatial scales of our selected astronomical sources, two different instruments have been used: the ALMA and the IRAM 30-m-diameter telescope. ALMA is an astronomical interferometer with 66 antennas

that is located in the Chajnantor Plateau at about 5000 m of elevation. ALMA operates at wavelengths from 3 to 0.3 mm. The IRAM 30 m telescope is a single-dish antenna located in Pico Veleta (Sierra Nevada, Spain). It operates at the 3, 2, 1, and 0.9 mm atmospheric bands that are transparent to external (sub)millimeter radiation coming from space. While single-dish antennas are typically used to observe extended astronomical sources in the sky such as the quiescent (and pc-scale**) GMC G + 0.693-0.027 in the Galactic Center, interferometers such as ALMA are needed to image with a high level of detail the molecular emission arising from the more compact sun-like protostars such as IRAS16293-2422 B (with a typical size of ~ 100 au[††]).

For the observations of the IRAS16293-2422 B hot corino, we have used several data sets obtained with ALMA in bands 3, 4, 6, 7, and 8, and which are publicly available from the ALMA data archive (Jørgensen *et al.*, 2016; Martín-Doménech *et al.*, 2017). The spectral line data cubes used for the identification of new molecular species and the determination of their abundances were obtained by subtracting the continuum emission in the uv-plane before doing the imaging by using line-free channels from the observed spectra. The standard ALMA calibration scripts and the Common Astronomy Software Applications package (McMullin *et al.*, 2007)[‡‡] were used for data calibration and imaging.

This data set covers a total bandwidth of ~ 14 GHz split into multiple spectral ranges between 86.5 and 353.5 GHz. The beam sizes range between 1.42″ and 1.85″ (equivalent to 200–260 au), while the spectral resolutions lie between 61 and 282 kHz corresponding to velocity resolutions of 0.1–0.9 km/s. For the analysis, we have considered a spatial circular support of 1.6″ diameter to extract the spectra from each spectral window toward the position of IRAS16293-2422 B: α(J2000.0) = 16 h 32 m 22.61 s, δ(J2000.0) = −24°28′32.″4400. Note that the beam sizes of the data set are larger than the size of source B (0.5″; Zapata *et al.*, 2013; Jørgensen *et al.*, 2016; Lykke *et al.*, 2017; Martín-Doménech *et al.*, 2017), and hence, the flux measured within our circular support of 1.6″ diameter contains all the flux independently of the beam. The beam sizes ≤1.9″ are sufficient to resolve source B from its companion source A in the IRAS16293-2422 binary, and therefore, the typical linewidths of the emission from IRAS16293-2422 B are ≤2 km/s.

The observations of the quiescent GMC G + 0.693-0.027 were carried out in April and August 2019 with the IRAM 30-m-diameter telescope located at Pico Veleta. The single-pointing coordinates of the source are α(J2000.0) = 17 h 47 m 22 s and δ(J2000.0) = −28°21′27.″ The position switching mode was used for observations and the coordinates of the reference position were α(J2000.0) = 17 h 46 m 23.01 s and δ(J2000.0) = −28°16′37.3.″

By using the broadband EMIR receivers, we observed the full 3 mm band (72–116 GHz) and partially covered the 2

**1 pc (or parsec) corresponds to 2×10^5 astronomical units (au) or 3×10^{13} km.

††1 au corresponds to 1.5×10^8 km.

‡‡https://casa.nrao.edu

and 1 mm bands (spectral ranges from 125 to 172 GHz, and from 208 to 238 GHz). The FTS200 mode of the backends was used, which provided spectral resolutions of ∼200 kHz, equivalent to 0.3–0.8 km/s between 72 and 238 GHz. To increase the signal-to-noise ratio in some parts of the survey, we smoothed the final reduced spectra to a frequency resolution of ∼400 kHz (*i.e.*, 0.6–1.6 km/s between 72 and 238 GHz). This velocity resolution is sufficient to resolve the typical linewidths of the molecular emission toward this source (∼20 km/s; Zeng *et al.*, 2018).

The half-power beam widths of the telescope were in the range ∼9″–35″ (equivalent to 8×10^4–3×10^5 au at the distance of the source of 8.5 kpc). Typical system temperatures, Tsys, ranged between 100 and 300 K in the 3, 2, and 1 mm atmospheric bands, respectively. The line intensity of our spectra is given in antenna temperature corrected for atmospheric attenuation, T_A^*, as the molecular emission toward G+0.693-0.027 is extended over the beam of the radio-telescope (Requena-Torres *et al.*, 2006; Martín *et al.*, 2008; Rivilla *et al.*, 2018).

We finally note that, for some species such as $CH_2(OH)$-CHO, we have used previous, less sensitive surveys on G+0.693-0.027 carried out with the IRAM 30 m telescope and the Green Bank Telescope. The details of these observations are described in detail in Zeng *et al.* (2018) and Rivilla *et al.* (2019b).

3. Results

3.1. Molecular line identification, T_{ex}, and molecular column densities

The line identification and analysis were performed with the MADCUBA (ImageJ) software package developed at the Center for Astrobiology in Spain (Rivilla *et al.*, 2016; Martin *et al.*, 2019). This software uses the spectroscopic data available from databases such as CDMS and JPL to carry out the transfer of a given species and for a given set of physical parameters such as molecular column density (N_{tot}), T_{ex}, central radial velocity (V_{LSR}), and linewidth (Δv). The MADCUBA-Spectral Line Identification and Modeling tool then produces synthetic spectra for each line profile by considering local thermodynamical equilibrium (LTE) and line opacity effects. The parameters are initially adjusted manually to match the synthetic spectra to the observed line profiles, and then, the MADCUBA-automatic fitting tool is finally used to provide the best nonlinear least-squared fit using the Levenberg–Marquardt algorithm.

In Tables 1 and 2 (see columns 3–6), we report the derived N_{tot} (and their 3σ upper limits in case of nondetections), T_{ex}, V_{LSR}, and Δv, obtained for our targeted molecules using this method. In Tables 6 and 7, we list the detected COM rotational transitions together with their quantum numbers, frequencies, line intensities at 300 K [$\log_{10} I(300 K)$], energies of the lower level (E_l), Δv, central radial velocities (V_{LSR}), and integrated intensities of the lines (Area). In Tables 6 and 7, we also include the transitions that have been used to estimate the upper limits to the column densities and abundances of the COMs that have not been detected in our observations.

We note that for the typical densities and linear scales imaged with ALMA toward the hot corino IRAS16293-2422, LTE is a good approximation (Jørgensen *et al.*, 2016). For the

quiescent GMC G+0.693-0.027, the low H_2 densities of the gas in this region ($\sim 10^4$ cm^{-3}; Rodríguez-Fernández *et al.*, 2004) could yield weak maser amplification in the molecular excitation of large COMs such as those studied here. However, those non-LTE effects appear at centimeter wavelengths (especially at frequencies <30 GHz) rather than in the millimeter range (Faure *et al.*, 2014, 2018).

The T_{ex} derived from the COM emission in this source are <15 K (Table 2; Requena-Torres *et al.*, 2006, 2008; Zeng *et al.*, 2018), which reflects the fact that these molecules are subthermally excited as a result of the low H_2 densities of the gas in this region. Since collisional rate coefficients with molecular H_2 are currently not available for these large COMs (collisional rate coefficients have been calculated only for methyl formate, CH_3OCHO, and methanimine, CH_2NH; Faure *et al.*, 2014, 2018), LTE analysis is the only method available to determine the excitation conditions of these COMs in the quiescent GMC G+0.693-0.027.

To calculate the molecular abundances relative to H_2, we consider an H_2 column density of 2.8×10^{25} cm^{-2} for IRAS16293-2422 as inferred by Martín-Doménech *et al.* (2017), and of 1.35×10^{23} cm^{-2} for G+0.693-0.027 as derived by Martin *et al.* (2008). The abundances (or upper limits) of all species are provided in column 7 of Tables 1 and 2.

From Figs. 2 and 3 and Tables 6 and 7, we find clear detections of ^{15}N isotopologue of HCN (HC^{15}N), $H_2C^{18}O/$ $H_2^{13}CO$, $HOCH_2CN$, $CH_2(OH)CHO$, NH_2CN, methanimine or CH_2NH, and E/Z-HNCHCN within the ALMA and IRAM 30 m datasets toward either or both astronomical sources. In addition, Fig. 4 and Table 7 report the detection of NH_2CONH_2 toward the quiescent GMC G+0.693-0.027. This represents the first detection of this prebiotic molecule outside a star-forming region (NH_2CONH_2 has recently been found for the first time toward the SgrB2 N massive hot core; Belloche *et al.*, 2019).

Table 7 lists the unblended transitions of NH_2CONH_2 measured toward G+0.693-0.027 (8 in total, but three are doublets). The observed intensities of the rest of transitions are consistent with our MADCUBA simulations because they are either blended with other molecular lines or fall below the rms noise level of our observations (typically of ∼3 mK in a velocity resolution of ∼1 km/s). Note that the transitions at 102.864 and 102.767 GHz (shown in Fig. 4) have been identified by Belloche *et al.* (2019) as clean from any molecular contaminant.

In addition, since the molecular excitation temperature in this source is $T_{ex} < 15$ K, we do not expect to detect many more low-excitation transitions of NH_2CONH_2 in the observed spectra besides those reported in Fig. 4 and Table 7. The spectrum of NH_2CONH_2 can be fitted well using an $T_{ex} = 8$ K (consistent with the T_{ex} measured for other COMs in this source; Requena-Torres *et al.*, 2006, 2008; Zeng *et al.*, 2018), and a column density of $(6.3 \pm 0.1) \times 10^{12}$ cm^{-2} (Fig. 4; Table 2). This implies an NH_2CONH_2 abundance of $\sim 5 \times 10^{-11}$ toward the quiescent GMC G+0.693-0.027. $CH_2(OH)CHO$, NH_2CN, methanimine, and E/Z-HNCHCN have been already reported by our group toward this source (Table 2; Requena-Torres *et al.*, 2008; Zeng *et al.*, 2018; Rivilla *et al.*, 2019b).

Our simulations with MADCUBA reveal that the isotopologues HC^{15}N, $H_2C^{18}O$ and $H_2^{13}CO$ are optically thin
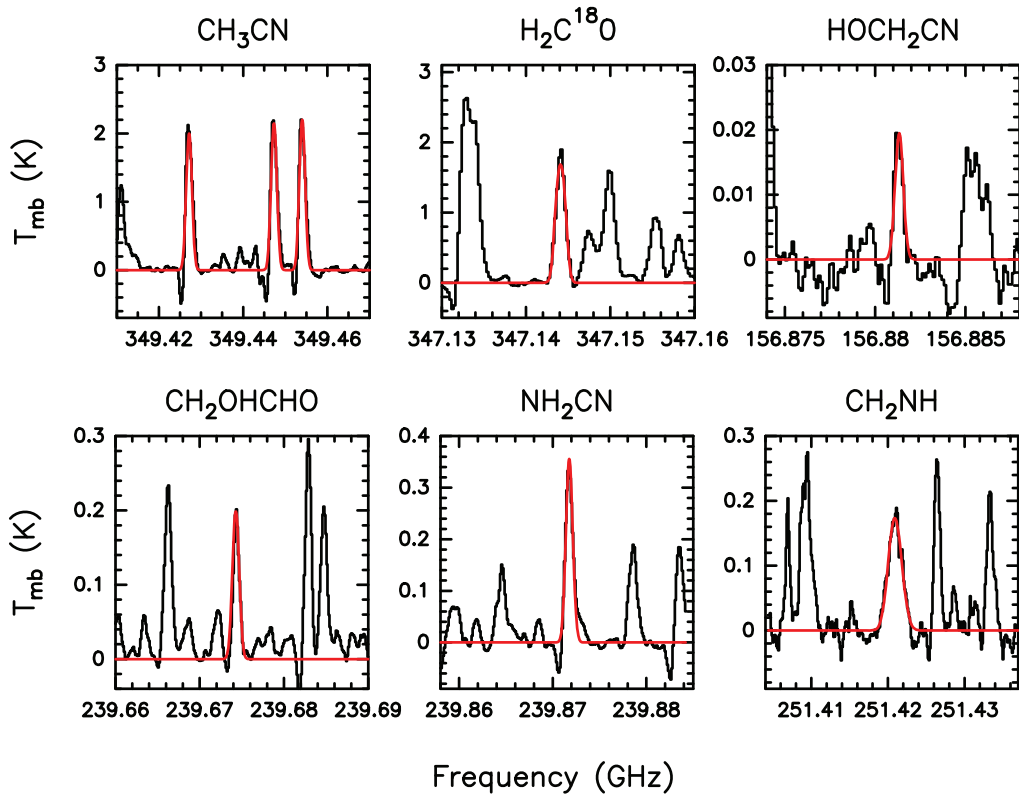
FIG. 2. Sample spectra of prebiotic species detected toward the IRAS16293-2422 B hot corino. Histograms correspond to some of the rotational transitions of COMs detected toward this proto-Sun, while red lines show the Gaussian fits to the observed line profiles performed by the MADCUBA-AUTOFIT tool. AUTOFIT, automatic fitting; COMs, complex organic molecules; MADCUBA, Madrid Data Cube Analysis. Color images are available online.
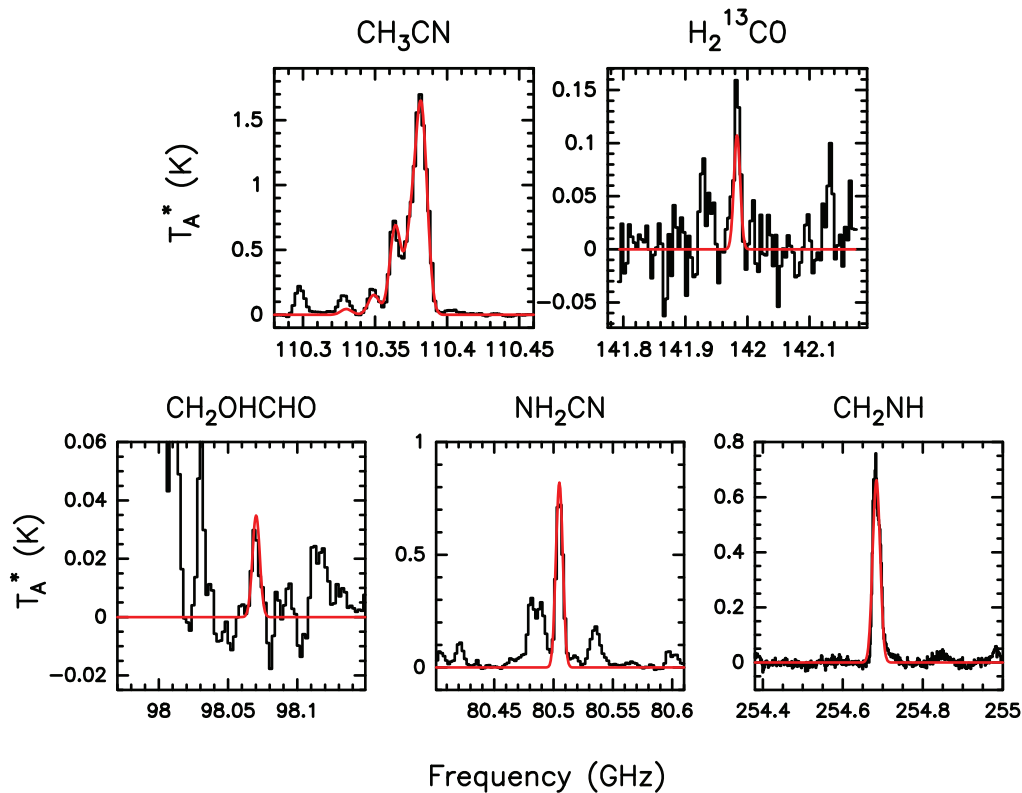
FIG. 3. Sample spectra of prebiotic species detected toward the quiescent GMC G+0.693-0.027. Histograms correspond to some of the rotational transitions of COMs detected toward this cloud in the Galactic Center, while red lines show the Gaussian fits to the observed line profiles obtained by MADCUBA. GMC, giant molecular cloud. Color images are available online.
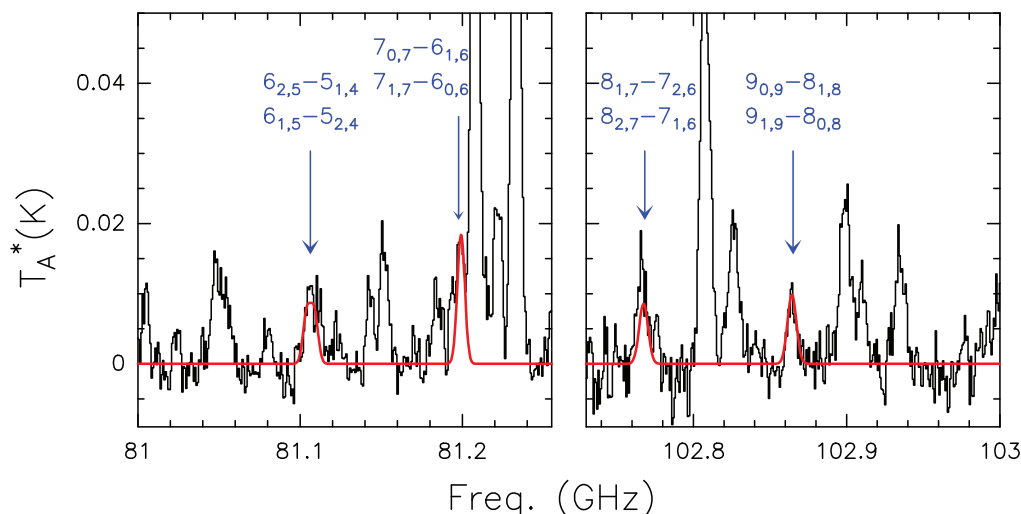
FIG. 4. Clean rotational transitions of urea detected toward G+0.693-0.027. Our IRAM 30 m observations cover 8 clean lines of urea, although three of them are doublets. This translates into five clear urea features detected in the observed spectra (see labeled lines). Red line indicates the spectrum of urea simulated with MADCUBA for a molecular column density of $(6.3 \pm 0.1) \times 10^{12}$ cm^{-2}, $T_{ex} = 8$ K, $\Delta v = 20$ km/s, and $V_{LSR} = 69$ km/s. IRAM, Instituto de Radioastronomía Milimétrica. Color images are available online.

toward IRAS16293-2422 B and G+0.693-0.027. Therefore, large optical depth effects do not likely affect their column densities reported in Tables 1 and 2.

Toward the proto-Sun IRAS16293-2422 B, CH$_2$(OH)-CHO, NH$_2$CN, and methanimine had been previously found by other groups; our derived column densities and excitation temperatures agree within factors of 10 and 2, respectively, with those inferred elsewhere (Bisschop *et al.*, 2008; Jørgensen *et al.*, 2016; Coutens *et al.* (2018b); Ligterink *et al.*, 2018; Persson *et al.*, 2018; Rivilla *et al.*, 2019a).

For HOCH$_2$CN and NH$_2$CN, these species are fitted better when using two temperature components along the line-of-sight, a hot (T > 100 K) and a cold (T < 30 K) component. These components are physically associated with the hot corino and the colder envelope around IRAS16293-2422 B, respectively, although in reality they may reflect a decreasing temperature gradient within the envelope of this source for increasing radii from the central protostar (see also Zeng *et al.*, 2019 for a detailed discussion on these two temperature components). In Table 1, however, we only present the results for the hot component associated with the hot corino. NH$_2$CONH$_2$ has not been detected toward the IRAS16293-2422 B hot corino, with a derived upper limit to its abundance of $\leq 2.3 \times 10^{-11}$.

The species CH$_2$OHCOOH, NH$_2$CH$_2$CN, CHOCHOH-CH$_2$OH, DHA-CH$_2$OHCOCH$_2$OH, NH$_2$CH$_2$COOH, and C$_3$H$_4$N$_2$O, have not been detected, so far, in any of the sources (see the upper limits to their derived column densities in column 6 of Tables 1 and 2). However, the unprecedented sensitivity of these observations provides stringent constraints to the upper limits of the abundances measured for these prebiotic COMs. Particularly stringent are the ones obtained toward G+0.693-0.027, thanks to our new high-sensitivity IRAM 30 m observations. These upper limits range between $\leq 0.4-17 \times 10^{-11}$ for CH$_2$OHCOOH, $\leq 0.4-5 \times 10^{-11}$ for NH$_2$CH$_2$CN, $\leq 5-9 \times 10^{-11}$ for CHOCHOHCH$_2$OH, $\leq 0.5-4 \times 10^{-10}$ for DHA, $\leq 2-4 \times 10^{-10}$ for NH$_2$CH$_2$COOH, and $\leq 1-8 \times 10^{-11}$ for C$_3$H$_4$N$_2$O.

3.2. Column density ratios of sugar-like species and N-bearing prebiotic COMs

In Tables 4 and 5, we report the column density ratios of sugar-like species (CH$_2$(OH)CHO, CH$_2$OHCOOH, CHO-CHOHCH$_2$OH, and DHA) with respect to H$_2$CO, and between N-bearing prebiotic species (HOCH$_2$CN, NH$_2$CN, methanimine, NH$_2$CONH$_2$, NH$_2$CH$_2$CN, HNCHCN, NH$_2$CH$_2$COOH, and C$_3$H$_4$N$_2$O) with respect to HCN. To calculate these ratios, we first need to derive the total

TABLE 4. COLUMN DENSITY RATIOS OF SUGAR-LIKE SPECIES WITH RESPECT TO FORMALDEHYDE

Molecule/H$_2$CO[a]	CH$_2$(OH)CHO	CH$_2$OHCOOH	CHOCHOHCH$_2$OH	DHA
IRAS16293-2422	0.01–0.02	$\leq 4 \times 10^{-5}$	$\leq 6 \times 10^{-4}$	≤ 0.004
G+0.693-0.027	0.08	≤ 0.06	≤ 0.03	≤ 0.017

We have obtained the ratios between the column densities of CH$_2$(OH)CHO, CH$_2$OHCOOH, CHOCHOHCH$_2$OH, and DHA with respect to H$_2$CO for both sources.

[a]The column density of H$_2$CO toward IRAS16293 is 2.8 10^{18} cm^{-2} and toward G+0.693-0.027, it is 4×10^{14} cm^{-2} (see text in Section 3.2 for the details on how these column densities have been calculated).

TABLE 5. COLUMN DENSITY RATIOS OF N-BEARING COMPLEX ORGANIC MOLECULES
WITH RESPECT TO (HYDROGEN CYANIDE)

Molecule/HCN[a]	HOCH$_2$CN	NH$_2$CN	CH$_2$NH	NH$_2$CONH$_2$	NH$_2$CH$_2$CN	HNCHCN	NH$_2$CH$_2$COOH	C$_3$H$_4$N$_2$O
IRAS16293-2422	∼0.03	∼0.009	∼0.07	≤0.01	≤0.002	≤0.002–0.02	≤0.1	≤0.005–0.02
G+0.693-0.027	≤0.001	0.05	0.08	0.001	≤0.0009	0.005–0.03	≤0.009	≤0.002

We have calculated the ratios of the column densities of HOCH$_2$CN, NH$_2$CN, CH$_2$NH, NH$_2$CONH$_2$, HNCHCN (E and Z), NH$_2$CH$_2$CN, NH$_2$CH$_2$COOH, and C$_3$H$_4$N$_2$O with respect to HCN for both astronomical sources.

[a]Column densities extracted from Tables 1 and 2; the estimated column densities for HCN are ∼6×10^{16} cm^{-2} toward IRAS16293-2422 B and >6.6×10^{15} cm^{-2} toward G+0.693-0.027.

column densities of H$_2$CO and HCN toward IRAS16293-2422 B and G+0.693-0.027.

H$_2$CO emission is optically thick toward both sources. However, we can use the optically thin isotopologues H$_2$C^{18}O toward IRAS16293-2422 B and H$_2^{13}$CO toward G+0.693-0.027. For IRAS16293-2422 B, we have assumed a ^{16}O/^{18}O isotopic ratio of ∼805 corresponding to that measured by Persson *et al.* (2018), while for G+0.693-0.027, we have considered a ^{12}C/^{13}C isotopic ratio of ∼20 as found in the Galactic Center (Wilson and Rood, 1994). Using these isotopic ratios, we derive H$_2$CO total column densities of 2.8×10^{18} cm^{-2} toward IRAS16293-2422 B and of 4×10^{14} cm^{-2} toward G+0.693-0.027. These H$_2$CO total column densities are similar to those estimated by Persson *et al.* (2018) for IRAS16293-2422 B (of 2×10^{18} cm^{-2}) and by Requena-Torres *et al.* (2006, 2008) toward G+0.693-0.027 (of 6.4×10^{14} cm^{-2}).

HCN emission is also optically thick toward both sources. To determine its column density, we use the HC^{15}N column densities provided in Tables 1 and 2. The HC^{15}N line observed with ALMA toward IRAS16293-2422 B shows an inverse P-Cygni profile with bright blue-shifted emission and a red-shifted component seen in absorption. This type of profile has already been observed toward this source in the spectra from other molecular species such as CH$_3$OCHO, CH$_3$OH, or HCO (Pineda *et al.*, 2012; Rivilla *et al.*, 2019a). The HC^{15}N line profile was fitted with the MADCUBA-AUTOFIT tool by assuming a source size of 0.5″ and an T$_{ex}$ = 150 K for the hot corino and by modeling the continuum emission using a modified black body with T$_c$ = 180 K, dust opacity index β = 0, and τ(94 GHz) = 2.1 (Rivilla *et al.*, 2019a).

For G+0.693-0.027, the HC^{15}N line only shows emission and it has been modeled without considering any continuum source. As isotopic ratios, we assume the ^{14}N/^{15}N ratio of ∼163–190 for IRAS16293-2422 B, that is, the same as the one measured by Wampfler *et al.* (2014) toward IRAS16293-2422 A. For G+0.693-0.027, we consider the lower limit to the ^{14}N/^{15}N ratio >600 obtained by Wilson and Rood (1994). The inferred total column densities of HCN are therefore $(5.7–6.7) \times 10^{16}$ cm^{-2} for IRAS16293-2422 B and >6.6×10^{15} cm^{-2} for G+0.693-0.027.

From Table 4, we obtain very stringent constraints to the abundance of sugar-like species relative to H$_2$CO: ∼1–2% for CH$_2$(OH)CHO, ≤0.004% for CH$_2$OHCOOH, ≤0.06% for CHOCHOHCH$_2$OH, and ≤0.4% for DHA in IRAS16293-2422 B; ∼8% for CH$_2$(OH)CHO, ≤6% for CH$_2$OHCOOH, ≤3% for CHOCHOHCH$_2$OH, and ≤1.7% for DHA in G+0.693-0.027. Interestingly, CH$_2$(OH)CHO, the only sugar-like species detected, presents column density ratios

of the same order toward IRAS16293-2422 B and G+0.693-0.027 (0.01–0.02 and 0.08, respectively), although it seems to be produced more efficiently in the quiescent Galactic Center GMC. One possible explanation is that the energetic processing of the gas and icy mantles of dust grains by shocks and/or cosmic rays in the Galactic Center favors the formation of sugar-like species such as CH$_2$(OH)CHO.

Indeed, it has been proposed that CH$_2$(OH)CHO formation is boosted by ice irradiation (Biver *et al.*, 2015). This irradiation can either be in the form of UV photons, X-rays, or cosmic rays, since all types of irradiation have the same effect on the final chemical composition of the ices (Muñoz Caro *et al.*, 2014; de Marcellus *et al.*, 2014; Meinert *et al.*, 2016; Ciaravella *et al.*, 2019). Although G+0.693-0.027 is not close to any obvious source of radiation, this cloud is embedded in an environment where the cosmic-ray ionization rate is enhanced by factors 100–1000 (Goto *et al.*, 2013). This yields an also enhanced radiation field of cosmic ray-induced, secondary UV-photons (by the same factors), which has a clear effect on the observed chemistry (Harada *et al.*, 2015; Zeng *et al.*, 2018). Therefore, the data presented here suggest that the formation of sugar-like species is boosted by irradiation in the ISM.

From Table 5, we find that HOCH$_2$CN is about 3% the amount of HCN measured in IRAS16293-2422 B, while it is undetected in the quiescent GMC G+0.693-0.027 (≤0.1% the amount of HCN). On the contrary, NH$_2$CN and HNCHCN are more abundant with respect to HCN in G+0.693-0.027 than in IRAS16293-2422 B (by factors of 5 and ≥1.5–2.5, respectively). The rest of N-bearing species show similar ratios toward both sources. Important upper limits to the abundance ratios with respect to HCN are those obtained for NH$_2$CH$_2$COOH (≤0.9%) and C$_3$H$_4$N$_2$O (≤0.2%; Table 5).

The different trends observed in the abundance ratios with respect to HCN for HOCH$_2$CN, and for NH$_2$CN and HNCHCN, may be related to the different chemistries found in these sources. G+0.693-0.027 is a turbulent GMC affected by large-scale shocks widespread across the Galactic Center, and by an enhanced cosmic ray ionization rate (Goto *et al.*, 2013; Harada *et al.*, 2015; Zeng *et al.*, 2019). The energetic processing of the molecular gas in this region favors the formation of unsaturated (hydrogen-poor) molecules such as NH$_2$CN and HNCHCN. In contrast, the chemistry in IRAS16293-2422 B is dominated by protostellar heating. During the warm-up phase, saturated (hydrogen-rich) species such as HOCH$_2$CN have enough time to form on the surface of dust grains (see the chemical modeling of HOCH$_2$CN for IRAS16293-2422 in Zeng *et al.*, 2019) and are thermally

TABLE 6. MOLECULAR ROTATIONAL TRANSITIONS OBSERVED TOWARD THE HOT CORINO
IRAS16293-2422 B AND REPORTED IN THIS WORK

Molecule name	Formula	Transition	Frequency (MHz)	Log_{10} [I(300 K)]	E_l (cm^{-1})	Δv (km/s)	V_{LSR} (km/s)	Area (Jy kms^{-1})
Hydrogen cyanide (^{15}N)	HC^{15}N	4–3	344,200.109	−2.72583	24.8	1.29±0.05	2.42±0.03	4.45±0.09
Formaldehyde (^{18}O)	H$_2$C^{18}O	$5_{0,5}$–$4_{0,4}$	345,881.039	−2.2054	23.1	0.98±0.06[b]	2.60±0.01[b]	2.98±0.06
		$5_{3,2}$–$4_{3,1}$	347,144.011	−2.0733	97.3	0.98±0.06[b]	2.60±0.01[b]	2.55±0.09
		$5_{2,3}$–$4_{2,2}$	348,032.433	−2.3444	56.2	0.98±0.06[b]	2.60±0.01[b]	2.05±0.03
		$5_{2,4}$–$4_{2,3}$	346,869.178	−2.3472	56.1	0.98±0.06[b]	2.60±0.01[b]	2.03±0.03
		$5_{4,1}$–$4_{4,0}$	346,984.094	−2.9202	155.0	0.98±0.06[b]	2.60±0.01[b]	0.26±0.02
		$5_{4,2}$–$4_{4,1}$	346,984.067	−2.9202	155.0	0.98±0.06[b]	2.60±0.01[b]	0.26±0.02
Cyanamide (hot)	NH$_2$CN	$12_{0,12}$–$11_{0,11}$	239,682.9192	−2.0556	93.5	1.03[a]	2.75±0.04[b]	0.20±0.01
		$12_{2,10}$–$11_{2,9}$	239,431.6816	−2.1594	132.8	1.03[a]	2.75±0.04[b]	0.16±0.01
		$12_{0,12}$–$11_{0,11}$	239,872.0312	−2.4181	44.0	1.03[a]	2.75±0.04[b]	0.09±0.01
		$12_{4,9}$–$11_{4,8}$	239,562.2461	−2.4349	250.4	1.03[a]	2.75±0.04[b]	0.08±0.01
		$12_{4,8}$–$11_{4,7}$	239,562.2462	−2.4349	250.4	1.03[a]	2.75±0.04[b]	0.08±0.01
		$12_{2,11}$–$11_{2,10}$	239,858.9859	−2.5145	84.3	1.03[a]	2.75±0.04[b]	0.07±0.01
		$12_{5,7}$–$11_{5,6}$	239,702.4999	−2.5467	295.0	1.03[a]	2.75±0.04[b]	0.06±0.01
		$12_{5,8}$–$11_{5,7}$	239,702.4999	−2.5467	295.0	1.03[a]	2.75±0.04[b]	0.06±0.01
		$12_{3,9}$–$11_{3,8}$	239,613.4863	−2.7462	181.9	1.03[a]	2.75±0.04[b]	0.04±0.01
		$12_{3,10}$–$11_{3,9}$	239,613.4863	−2.7462	181.9	1.03[a]	2.75±0.04[b]	0.04±0.01
		$12_{4,9}$–$11_{4,8}$	239,805.2745	−2.8038	204.9	1.03[a]	2.75±0.04[b]	0.04±0.01
		$12_{4,8}$–$11_{4,7}$	239,805.2745	−2.8038	204.9	1.03[a]	2.75±0.04[b]	0.04±0.01
Methanimine	CH$_2$NH	$6_{0,6}$–$5_{1,5}$	251,421.178	−2.8996	36.1	2.0±0.9	3.3±0.3	0.44±0.04
Glycolic acid	CH$_2$OHCOOH	$37_{4,33}$–$36_{4,32}$	247,406.9484	−3.5061	161.0	1.03[a]	2.52[a]	≤0.003
Urea	NH$_2$CONH$_2$	$14_{1,14}$–$13_{0,13}$	157,024.1234	−3.1113	35.2	1.03[a]	2.52[a]	≤0.03
		$14_{0,14}$–$13_{1,13}$	157,024.1234	−3.1113	35.2	1.03[a]	2.52[a]	≤0.03
E-cyanomethanimine	E-HNCHCN	$25_{4,22}$–$24_{4,21}$	239,583.436	−2.6463	126.7	1.03[a]	2.52[a]	≤0.013
Z-cyanomethanimine	Z-HNCHCN	$25_{4,21}$–$24_{4,20}$	243,136.2686	−3.4159	123.5	1.03[a]	2.52[a]	≤0.03
Aminoacetonitrile	NH$_2$CH$_2$CN	$38_{3,36}$–$37_{3,35}$	342,845.8958	−2.7264	220.4	1.03[a]	2.52[a]	≤0.013
Glyceraldehyde	CHOCHO-HCH$_2$OH	$24_{7,17}$–$23_{6,17}$	157,134.1516	−4.3181	51.9	1.03[a]	2.52[a]	≤0.005
Dihydroxyacetone (DHA)	CH$_2$OHCO-CH$_2$OH	$26_{7,20}$–$26_{6,21}$	101,268.1871	−5.23	54.0	1.03[a]	2.52[a]	≤0.003
Glycine	NH$_2$CH$_2$COOH	$35_{9,26}$–$34_{9,25}$	252,275.3207	−4.1826	156.7	1.03[a]	2.52[a]	≤0.02
2-Amino-oxazole 0$^+$	C$_3$H$_4$N$_2$O 0$^+$	$19_{19,1}$–$18_{18,0}$	348,360.1687	−3.7665	102.8	1.03[a]	2.52[a]	≤0.006
		$19_{19,0}$–$18_{18,1}$	348,360.1687	−3.7665	102.8	1.03[a]	2.52[a]	≤0.006
2-Amino-oxazole 0$^-$	C$_3$H$_4$N$_2$O 0$^-$	$28_{14,14}$–$27_{13,15}$	348,375.6632	−3.9458	118.8	1.03[a]	2.52[a]	≤0.012
		$28_{14,15}$–$27_{13,14}$	348,375.4669	−3.9458	118.8	1.03[a]	2.52[a]	≤0.012

[a]Δv and V$_{LSR}$ fixed in MADCUBA.
[b]Δv and V$_{LSR}$ are the same for all transitions from the same molecule when simulating the spectra within MADCUBA.

sublimated and incorporated into the gas phase once the temperature of the dust reaches 100 K (*i.e.*, the desorption temperature for water; Collings *et al.*, 2004).

4. Discussion

4.1. Comparison with previous searches of large prebiotic COMs: NH$_2$CH$_2$COOH, DHA, and CHOCHOHCH$_2$OH

Because of its simplicity, NH$_2$CH$_2$COOH has been the only amino acid extensively searched for in the ISM. Deep searches have been carried out toward a variety of astronomical objects such as massive hot cores (*e.g.*, in SgrB2, Orion KL, W51 e1/e2; Kuan *et al.*, 2003; Belloche *et al.*, 2013, 2008), low-mass hot corinos (as in IRAS16293-2422; Ceccarelli *et al.*, 2000), and prestellar cores (L1544; Jiménez-Serra *et al.*, 2016), but all of them have been unsuccessful. The upper limit derived in this work for NH$_2$CH$_2$COOH toward the hot corino in IRAS16293-

2422 B (≤2.1×10^{-10}; Table 1) is a factor ≥30 lower than that previously reported by Ceccarelli *et al.* (2000; of ≤7×10^{-9}). This implies that the amount of NH$_2$CH$_2$COOH formed in the ices during the warming up of the protostellar envelope is ≤0.0003% the abundance of water, assuming all ice content has been released into the gas phase in the hot corino evaporation phase and considering a water abundance of 7.25×10^{-5} with respect to H$_2$ (Whittet and Duley, 1991). This low relative abundance of NH$_2$CH$_2$COOH with respect to water is a factor of ~50 lower than that obtained in UV-irradiated interstellar ice analogues (NH$_2$CH$_2$COOH abundance of ~10^{-4} with respect to water, or ~10^{-8} with respect to H$_2$; Muñoz Caro *et al.*, 2002), and it is consistent with the abundance range inferred by Rosetta Orbiter Spectrometer for Ion and Neutral Analysis in comet 67P/Churyumov–Gerasimenko (between 0 and 0.0025 with respect to water; Altwegg *et al.*, 2016).

Irradiation can yield a wide variety of amino acids in ices under interstellar conditions (Bernstein *et al.*, 2002;

TABLE 7. MOLECULAR ROTATIONAL TRANSITIONS OBSERVED TOWARD THE QUIESCENT GIANT
MOLECULAR CLOUD G+0.693-0.027 AND REPORTED IN THIS WORK

Molecule name	Formula	Transition	Frequency (MHz)	Log_{10} [I(300 K)]	E_l (cm^{-1})	Δv (km/s)	V_{LSR} (km/s)	Area (K kms^{-1})
Formaldehyde (^{13}C)	H$_2^{13}$CO	$2_{0,2}-1_{0,1}$	141,983.7404	−3.3163	2.4	19.8±0.2[b]	70.4±0.1[b]	4.16±0.09
		$3_{0,3}-2_{0,2}$	212,811.184	−2.801	7.1	19.8±0.2[b]	70.4±0.1[b]	2.21±0.04
Glycolonitrile	HOCH$_2$CN	$8_{1,7}-7_{1,6}$	75,463.333	−4.632	9.8	...	...	≤0.05
Glycolaldehyde	CH$_2$(OH)CHO	$3_{3,0}-2_{2,1}$	98,070.5113	−4.6328	2.8	20[a]	70[a]	0.45±0.2
		$3_{3,1}-2_{2,0}$	97,919.5791	−4.6335	2.9	20[a]	70[a]	0.45±0.2
		$4_{3,1}-3_{2,2}$	109,877.1408	−4.5319	4.0	20[a]	70[a]	0.40±0.2
		$5_{4,1}-4_{3,2}$	146,445.05	−4.1447	7.7	20[a]	70[a]	0.32±0.2
		$5_{2,3}-4_{1,4}$	107,886.2448	−4.9176	4.0	20[a]	70[a]	0.32±0.2
Glycolic acid	CH$_2$OHCOOH	$11_{2,10}-10_{2,9}$	74,028.9895	−4.7706	19.0	20[a]	70[a]	≤0.05
Urea	NH$_2$CONH$_2$	$7_{1,7}-6_{0,6}$	81,199.2	−3.9453	8.7	20[a]	69[a]	0.20±0.02
		$7_{0,7}-6_{1,6}$	81,199.2	−3.9453	8.7	20[a]	69[a]	0.20±0.02
		$6_{1,5}-5_{2,4}$	81,104.13	−4.1074	7.9	20[a]	69[a]	0.15±0.02
		$6_{2,5}-5_{1,4}$	81,108.77	−4.1074	7.9	20[a]	69[a]	0.15±0.02
		$9_{1,9}-8_{0,8}$	102,864.32	−3.6353	14.4	20[a]	69[a]	0.11±0.02
		$9_{0,9}-8_{1,8}$	102,864.32	−3.6353	14.4	20[a]	69[a]	0.11±0.02
		$8_{2,7}-7_{1,6}$	102,767.56	−3.7539	13.7	20[a]	69[a]	0.09±0.02
		$8_{1,7}-7_{2,6}$	102,767.56	−3.7539	13.7	20[a]	69[a]	0.09±0.02
Glyceraldehyde	CHOCHOH-CH$_2$OH	$8_{7,1}-7_{6,1}$	78,879.586	−5.1099	8.3	20[a]	69[a]	≤0.02
		$8_{7,2}-7_{6,2}$	78,879.586	−5.1099	8.3	20[a]	69[a]	≤0.02
Dihydroxyacetone (DHA)	CH$_2$OHCO-CH$_2$OH	$5_{5,1}-4_{4,0}$	90,104.154	−5.714	5.5	20[a]	69[a]	≤0.014
		$5_{5,0}-4_{4,1}$	90,104.154	−5.714	5.5	20[a]	69[a]	≤0.014
Glycine (conformer I)	NH$_2$CH$_2$COOH	$4_{4,1}-3_{3,0}$	75,795.2729	−6.2317	3.4	20[a]	69[a]	≤0.03
2-Amino-oxazole 0$^+$	C$_3$H$_4$N$_2$O 0$^+$	$5_{4,2}-4_{3,1}$	75,299.4615	−5.6144	4.0	20[a]	69[a]	≤0.03
2-Amino-oxazole 0$^-$	C$_3$H$_4$N$_2$O 0$^-$	$5_{4,2}-4_{3,1}$	75,273.6888	−5.6146	4.0	20[a]	69[a]	≤0.03

[a]Δv and V_{LSR} fixed in MADCUBA.
[b]Δv and V_{LSR} are the same for all transitions from the same molecule when simulating the spectra within MADCUBA.

Muñoz Caro *et al.*, 2002). However, the upper limit to the abundance of NH$_2$CH$_2$COOH measured toward the quiescent GMC G+0.693-0.027 gives an abundance of ≤4×10^{-10} or ≤0.0006% with respect to water (Table 2). As mentioned in Section 3.2, the GMC G+0.693-0.027 is located in the Galactic Center and it is affected by enhanced cosmic ray ionization rates. Since both UV and cosmic ray irradiations yield a similar chemistry and COM composition in interstellar ices (Muñoz Caro *et al.*, 2014), our measured upper limit to the abundance of NH$_2$CH$_2$COOH suggests that ice irradiation may not produce NH$_2$CH$_2$COOH efficiently in the ISM. Alternatively, this molecule could form on irradiated interstellar ices but, once injected into the gas phase by protostellar feedback, NH$_2$CH$_2$COOH could be destroyed quickly by ions and radicals (Garrod, 2013; Suzuki *et al.*, 2018).

In contrast to NH$_2$CH$_2$COOH, DHA and CHOCHOH-CH$_2$OH have only been searched for toward the SgrB2 N-LMH massive hot core (Hollis *et al.*, 2004; Widicus Weaver and Blake, 2005; Apponi *et al.*, 2006). For DHA, Widicus Weaver and Blake (2005) reported a tentative detection of this large prebiotic COM through measurements of nine possible rotational transitions of this molecule with the Caltech Submillimeter Observatory telescope. The inferred abundance of DHA in this source is 1.2×10^{-9}. This tentative detection has never been confirmed (Apponi *et al.*, 2006), which is in line with our findings. The derived upper limits to the abundance of DHA in IRAS16293-2422 B and G+0.693-0.027 range from ≤1.8 to 3.9×10^{-10}, that is,

factors 3–7 lower than the abundance measured in SgrB2 N-LMH by Widicus Weaver and Blake (2005).

For CHOCHOHCH$_2$OH, Hollis *et al.* (2004) reported just upper limits to the abundance of this molecule, which is consistent with our nondetection (upper limit to the abundance of CHOCHOHCH$_2$OH of ≤2.4–5.7×10^{-11}; Tables 1 and 2). This implies that the so-called formose reaction, by which H$_2$CO polymerizes on interstellar dust grains into CH$_2$(OH)CHO first and then into CHOCHOHCH$_2$OH and into more complex sugars (Larralde *et al.*, 1995), does not seem to operate in the ISM.

4.2. Comparison with the COM content in comets

One possible scenario for the appearance of prebiotic material on a young Earth is the delivery of such material by the impact of comets and/or meteorites on Earth's surface. It is currently believed that the COM content in comets is directly linked to the pristine chemical composition of the solar nebula, that is, to the chemical composition developed during the first stages of low-mass star formation. This is supported by the high deuterium enrichment measured in comets, which can only be explained if the composition of their icy surfaces was set in the presolar cloud at large distances from the Sun (Ceccarelli *et al.*, 2014; Altwegg *et al.*, 2015). Therefore, the comparison between the prebiotic COM content in comets and in the ISM can provide insight into how life originated on the Earth.

HCN and H_2CO are among the most abundant species in comets such as C/2014 Q2 Lovejoy (Biver *et al.*, 2015) and 67P/Churyumov–Gerasimenko (Goesmann *et al.*, 2015). We have thus calculated the COM ratios (with respect to HCN and H_2CO) available in the literature and compared them with the ones provided in Tables 4 and 5. For sugar-like species, the $CH_2(OH)CHO/H_2CO$ abundance ratio is ~ 0.05 in comet C/2014 Q2 Lovejoy, as inferred from their relative abundances to water reported in Table 1 of Biver *et al.* (2015). This ratio falls within the range of the $CH_2(OH)$-CHO/H_2CO ratios measured toward IRAS16293-2422 B (0.01–0.02) and G+0.693-0.027 (0.08; Table 4). The slightly higher abundance of $CH_2(OH)CHO$ in comets with respect to the hot corino stage (Table 4; figure 2 in Biver *et al.*, 2015) can be attributed to the synthesis of this sugar-like species through grain-surface reactions and subsequent ice irradiation in the solar nebula. This idea is supported by the higher $CH_2(OH)CHO/H_2CO$ ratio measured toward G+0.693-0.027, which is exposed to the enhanced cosmic-ray ionization rates of the Galactic Center.

For N-bearing prebiotic species, the abundance ratio of NH_2CH_2COOH/HCN measured in comet 67P/Churyumov–Gerasimenko is ~ 0.003, which is consistent with the upper limits obtained toward the two sources (≤ 0.1 for IRAS16293-2422 B and ≤ 0.009 for G+0.693-0.027). This suggests that the COM material in comets could have an ISM origin. Unfortunately, NH_2CH_2COOH is the only N-bearing molecule from our list of prebiotic species for which comet data are available. Additional remote observations of species such as $HOCH_2CN$, NH_2CN, or methanimine toward comets are needed to better characterize the link between the N-bearing COM prebiotic content in these objects and that of the ISM.

4.3. NH_2CONH_2 as a common prebiotic product of ISM chemistry

NH_2CONH_2 is a key molecule in animal life because it plays an important role in the metabolism of N-containing compounds. Until recently, the detection of NH_2CONH_2 had remained elusive. However, Belloche *et al.* (2019) have reported the first detection of this prebiotic species in the ISM toward the hot molecular envelope around a massive(s) protostar (the SgrB2 N hot core; Belloche *et al.*, 2019). Our high-sensitivity observations, carried out with the IRAM 30 m telescope toward the quiescent GMC G+0.693-0.027, not only provide the second detection of NH_2CONH_2 in space (with a derived abundance of 4.7×10^{-11}) but also show that this molecule can be formed in the ISM in regions unaffected by star formation.

Belloche *et al.* (2019) did not provide any absolute abundance of NH_2CONH_2 in their work and therefore a direct comparison with the NH_2CONH_2 abundance estimated toward G+0.693-0.027 cannot be performed. However, we can check the relative abundance of this prebiotic molecule with respect to other chemically related species such as CH_3NCO and NH_2CHO (Belloche *et al.*, 2019). Using the column densities of CH_3NCO and NH_2CHO derived toward G+0.693-0.027 by Zeng *et al.* (2018), we infer that the NH_2CONH_2/CH_3NCO and NH_2CONH_2/NH_2CHO column density ratios are ~ 0.1 and ~ 0.01, respectively. From Table 4 of Belloche *et al.* (2019), we can calculate the same column density ratios toward the massive hot core SgrB2 N1, which gives ~ 0.11 for NH_2CONH_2/CH_3NCO

and ~ 0.009 for NH_2CONH_2/NH_2CHO. These ratios are very similar to the ones found in G+0.693-0.027. This suggests that the chemistry of NH_2CONH_2 likely follows similar formation/destruction pathways both in hot cores and in Galactic Center-quiescent GMCs.

Belloche *et al.* (2019) proposed that NH_2CONH_2 is formed directly from NH_2CHO on the surface of dust grains. The process starts with the abstraction of H from NH_2CHO, which yields the intermediate species NH_2CO that is then free to react with NH_2 to form NH_2CONH_2. This scenario is supported by recent laboratory experiments of UV irradiation of $CH_4:HNCO$ ice mixtures (Ligterink *et al.*, 2018), which produce the intermediate radical NH_2CO in high amounts. Alternatively, NH_2CONH_2 could be formed in the ISM via the gas-phase reaction $NH_2OH_2^+ + NH_2CHO$, although, as recently shown by Jeanvoine and Spetia (2019), this reaction does not proceed under interstellar conditions.

From all this, NH_2CONH_2 formation seems to be dependent on the production of NH_2CHO. According to our results, the formation yield of NH_2CONH_2 is 1% that of NH_2CHO. The production of NH_2CHO in the ISM has been the subject of debate in recent years. Some groups have proposed that NH_2CHO is formed on the surface of dust grains (Fedoseev *et al.*, 2016; Dulieu *et al.*, 2019), while others suggest that NH_2CHO is produced by pure gas-phase reactions such as $NH_2 + H_2CO \rightarrow NH_2CHO + H$ (Skouteris *et al.*, 2017). Alternatively, Quénard *et al.* (2018) have proposed that the production of NH_2CHO may be a combination of the two processes (gas-phase and grain surfaces), each of them dominating at different physical regimes. For the physical conditions found in hot molecular cores and in the Galactic Center-quiescent GMCs, grain surface formation dominates, which explains why the NH_2CONH_2/NH_2CHO column density ratios measured toward SgrB2 N1 and G+0.693-0.027 are very similar. Further laboratory experiments and theoretical calculations are needed to expand our understanding on the chemistry of NH_2CONH_2 in the ISM.

4.4. The missing link: $C_3H_4N_2O$

In the RNA-world chemical scheme, $C_3H_4N_2O$ plays a central role in the formation of pyrimidine ribonucleotides (Powner *et al.*, 2009; Patel *et al.*, 2015; Fig. 1). In this work, we have presented the first attempt to detect this large COM in the ISM. The derived upper limits to its abundance (for both states 0^+ and 0^-) toward IRAS16293-2422 B and G+0.693-0.027 are $\leq (1-8) \times 10^{-11}$ with respect to H_2 or $\leq 0.002-0.02$ with respect to HCN. The lack of detection may be due to two reasons: (1) the transitions covered within our observations may not have been the most favorable for a detection experiment; or (2) the sensitivity of the observations is not high enough for a detection experiment of $C_3H_4N_2O$ in the ISM.

To check case (1), we simulated the spectrum of 2-amino-oxazol (for both states 0^+ and 0^-) using MADCUBA and considering the physical conditions and the upper limits to the abundance of $C_3H_4N_2O$ measured in IRAS16293-2422 B and G+0.693-0.027. When the excitation temperature of the gas (T_{ex}) is low (of ~ 10 K, as in G+0.693-0.027), the brightest lines of $C_3H_4N_2O$ 0^+ and 0^- appear at frequencies 87,273/87,300 MHz and 105,921/105,952 MHz (*i.e.*, the $5_{5,K2}-4_{4,K2'}$ and $6_{6,K2}-5_{5,K2'}$ transitions of the $0^-/0^+$ states, respectively). These transitions were covered with the IRAM 30 m telescope toward G+0.693-0.027. However, for an $T_{ex}=150$ K (as

assumed for most COM materials in IRAS16293-2422 B), the brightest lines of $C_3H_4N_2O$ should be found at 256,585/256,670 MHz (the $16_{13,K2}$-$15_{12,K2'}$ transitions of the $0^-/0^+$ states, respectively). These transitions are not included in the ALMA data set used here.

To test case (2), the upper limits to the abundance of $C_3H_4N_2O$ are still high since the lowest values measured in the ISM for the abundance of COMs are of the order of $\sim 10^{-12} - 10^{-13}$ (Jiménez-Serra et al., 2016). Therefore, while for G+0.693-0.027, the nondetection of $C_3H_4N_2O$ may have been related to the lack of sensitivity, for IRAS16293-2422 B, it may have been due to both poor sensitivity and lack of bright-enough transitions covered within the observations.

4.5. Evolution of astrochemistry and prebiotic chemistry: toward astrobiochemistry in the ISM

The first experiments of prebiotic chemistry used simple molecules such as H_2O, CH_4, NH_3, or HCN as precursors of proteinogenic amino acids (such as NH_2CH_2COOH and alanine) and of simple nucleobases (such as adenine; Miller, 1953; Oró and Kimball, 1961). The use of these simple species was motivated by their early discovery in space (Cheung et al., 1969; Snyder and Buhl, 1971). However, subsequent studies showed that early Earth's atmosphere may have been richer in other gases such as CO_2 or N_2 rather than H_2O or NH_3; and in addition, although amino acids are formed in the Miller–Urey experiment, they cannot be assembled spontaneously into polypeptide chains (i.e., proteins) without the intervention of RNA, which led researchers to propose the RNA-world scenario for the origin of life (see review by, e.g., Ruiz-Mirazo et al., 2014).

The chemical scheme of Powner et al. (2009) uses more complex molecules such as NH_2CN or $CH_2(OH)CHO$ as precursors of the RNA formation process. This may have been a conceptual problem in the 70s and 80s, because these molecules (believed to be injected into a young Earth through the impact of comets and meteorites on Earth's surface) were unknown in the ISM.

In the past decade, however, astrochemistry has been extremely successful at detecting new COMs in space, which demonstrates the increasingly high level of chemical complexity found in the ISM (Herbst and van Dishoeck, 2009). Indeed, COMs such as NH_2CN and $CH_2(OH)CHO$ are nowadays routinely detected across multiple environments in the ISM (e.g., low-mass and high-mass protostars, galactic center GMCs; Requena-Torres et al., 2008; Jorgensen et al., 2012; Coutens et al., 2018; Zeng et al., 2018). In addition, our recent discoveries of $HOCH_2CN$ and Z-HNCHCN (a precursor of adenine) toward the hot corino IRAS16293-2422 B and the quiescent GMC G+0.693-0.027 in the Galactic Center, respectively (Rivilla et al., 2019b; Zeng et al., 2019), as well as the detection of NH_2CONH_2 (Belloche et al., 2019; this work), not only demonstrate the wide variety of chemical compounds that can be formed under interstellar conditions but also show that ISM chemistry, by itself, tends to form precursors that are essential for the synthesis process of RNA. This means that if these compounds were delivered to the surface of a young planet by the impact of comets and/or meteorites, they could trigger downstream in the chemical scheme of Patel et al. (2015), the production chain of ribonucleotides in aqueous solution without having to invoke the first reactions.

Our analysis below shows that the reaction formation/destruction processes of these prebiotic species are very different in space from those occurring in aqueous solutions. However, our intention in this work is to show that, if they were injected early into the reaction network of the primordial RNA-world chemical scheme of Patel et al. (2015), they would facilitate the subsequent production of ribonucleotides. Indeed, experiments of simulated meteorite impacts of prebiotic species such as $CH_2(OH)CHO$ mixed with clay reveal that these COM molecules not only survive the impact but they also react forming new biologically relevant molecules (McCaffrey et al., 2014).

The different reaction processes involved in the formation/destruction of prebiotic species in the ISM and in aqueous solution become apparent if one pays attention to the molecular abundances derived for these precursors toward IRAS16293-2422 B and G+0.693-0.027. Tables 1 and 2 show that $HOCH_2CN$ (a key precursor of $CH_2(OH)CHO$ in the chemical scheme proposed by Patel et al., 2015) is at least one order of magnitude less abundant than $CH_2(OH)CHO$. In fact, $HOCH_2CN$ is not even detected toward G+0.693-0.027, which contrasts the relatively high abundance of $CH_2(OH)CHO$ measured toward this source ($\sim 3 \times 10^{-10}$). This rules out $HOCH_2CN$ as a precursor of $CH_2(OH)CHO$ in space.

The formation of $CH_2(OH)CHO$ in the ISM has remained a mystery for a long time since this species tends to be more abundant in regions with temperatures colder than those found in hot cores. This is the case of the line-of-sight toward the hot molecular core SgrB2 N, where $CH_2(OH)CHO$ presents a higher abundance in the molecular envelope than in the hot core (Hollis et al., 2000). One possibility is that $CH_2(OH)CHO$ is formed in the gas phase from COM precursors such as methanol or formic acid (in their protonated forms; Laas et al., 2011) or ethanol (Skouteris et al., 2018). However, recent chemical modeling and observations suggest that $CH_2(OH)CHO$ may form more efficiently on the surface of dust grains via either the dimerization of HCO followed by hydrogenation or the reaction between the radicals HCO and CH_2OH (Woods et al., 2013; Rivilla et al., 2017, 2019a; Coutens et al. (2018a). The observed trend for the abundance ratio between ethylene glycol and glycolaldehyde to increase with increasing luminosity supports the grain surface formation route for $CH_2(OH)CHO$ (Coutens et al., 2018a; Rivilla et al., 2019a).

For NH_2CN, this molecule is a factor of 10 less abundant than methanimine (at least toward IRAS16293-2422 B, a proto-Sun), which suggests that the latter species may be the actual precursor of larger amine COMs (Coutens et al., 2018b).

From Tables 1 and 2, it is clear that the derived upper limits to the abundance of key species in the chemical scheme of the RNA-world scenario, such as $C_3H_4N_2O$, $CHOCHOHCH_2OH$, or DHA, are still high (between 10^{-11} and 10^{-10}). These upper limits therefore do not allow us to rule out the possibility that these species are not present in the ISM. Particularly important is the molecule $C_3H_4N_2O$, which is a bottleneck in the pyrimidine nucleotide formation process (Powner et al., 2009).

We note that besides $CHOCHOHCH_2OH$ and DHA, other interesting sugars are ribose, ribofuranoside, or deoxyribose, for which their rotational spectra have been recently

measured and characterized in the laboratory (Cocinero *et al.*, 2012; Peña *et al.*, 2013; Écija *et al.*, 2016). Toward astronomical sources with low excitation temperatures of the gas such as the quiescent GMC G+0.693-0.027, the peak of the spectra of these prebiotic COMs shifts to frequencies between 30 and 80 GHz. This frequency range is better suited for the detection of these complex organics because the observed spectra are cleaner from rotational transitions from lighter molecular species, and because the frequency span between transitions is larger, which diminishes the effects of line confusion (Jiménez-Serra *et al.*, 2014). Therefore, future instrumentation such as the band 1 and 2 receivers of ALMA, the K and Q bands of the Next-Generation Very Large Array, and the band 5 receivers of the Square Kilometer Array, will be key in the search of prebiotic COMs in the ISM.

5. Conclusions

Since the first prebiotic experiments of Miller–Urey and Joan Oro based on simple molecules detected in the ISM, astrochemistry has evolved and shown the presence of a wealth of complex organic compounds that can be formed in the ISM with relatively high abundances. The recent discovery in the ISM of prebiotic COMs such as $CH_2(OH)$-CHO, $HOCH_2CN$, HNCHCN, and NH_2CONH_2, precursors of ribonucleotides, and more complex sugars, might support the hypothesis of a primordial RNA-world in a young Earth.

In this study, we present a detailed study of the abundances of the precursors of the proposed RNA-world chemical scheme, toward a massive cloud in the center of our galaxy (the quiescent GMC G+0.693-0.027) and a star-forming region in the disk of the Milky Way (the hot corino IRAS16293-2422 B). Our high-sensitivity observations toward the quiescent GMC G+0.693-0.027 have revealed the presence of NH_2CONH_2 also in this source not affected by star formation with an abundance $\sim 5 \times 10^{-11}$.

We have also searched for other key molecules in the RNA-world scenario such as $C_3H_4N_2O$, CHOCHOH-CH_2OH, and DHA, toward both astronomical sources, but these searches have yielded no detection so far. We derive the upper limits to the abundance of these species and conclude that, although the ISM is an efficient factory in the production of COMs and of key prebiotic precursors compatible with a primordial RNA-world, the chemical pathways used by the ISM for the formation of these precursors largely differ from those proposed in the works of Powner *et al.* (2009) and Patel *et al.* (2015). In any case, the potentially efficient production in the ISM of these key prebiotic precursors opens the possibility for the RNA-world prebiotic chemistry to develop elsewhere in the Universe.

Acknowledgments

Author Disclosure Statement

No competing financial interests exist.

Funding Information

Supplementary Material

Supplementary Data

References

Adams, F.C. (2010) The Birth Environment of the Solar System. *ARA&A* 48:47.

Altwegg, K., Balsiger, H., Bar-Nun, A., Berthelier, J.J., Bieler, A., Bochsler, P., Briois, C., Calmonte, C., Combi, M., De Keyser, J., Eberhardt, P., Fiethe, B., Fuselier, S., Gasc, S., Gombosi, T.I., Hansen, K.C., Hässig, M., Jäckel, A., Kopp, E., Korth, A., LeRoy, L., Mall, U., Marty, B., Mousis, O., Neefs, E., Owen, T., Rème, H., Rubin, M., Sémon, T., Tzou, C.Y., Waite, H., and Wurz, P. (2015) 67P/Churyumov–Gerasimenko, a Jupiter family comet with a high D/H ratio. *Science* 347:6220.

Altwegg, K., Balsiger, H., Bar-Nun, A., Berthelier, J.J., Bieler, A., Bochsler, P., Briois, C., Calmonte, U., Combi, M., Cottin, H., De Keyser, J., Dhooghe, F., Fiethe, B., Fuselier, S., Gasc, S., Gombosi, T., Hansen, K., Haessig, M., Jäckel, A., Kopp, E., Korth, A., Le Roy, L., Mall, U., Marty, B., Mousis, O., Owen, T., Rème, H., Rubin, M., Sémon, T., Tzou, C., Hunter Waite, J., and Wurz, P. (2016) Prebiotic chemicals—amino acid and phosphorus—in the coma of comet 67P/Churyumov–Gerasimenko. *Sci Adv* 2:e1600285.

Apponi, A.J., Halfen, D.T., Ziurys, L.M., Hollis, J.M., Remijan, A.J., and Lovas, F.J. (2006) Investigating the limits of chemical complexity in Sagittarius B2(N): a rigorous attempt to confirm 1,3-dihydroxyacetone. *Astrophys J* 643:L29–L32.

Belloche, A., Menten, K., Comito, C., Müller, H., Schilke, P., Ott, J., Thorwirth, S., and Hieret, C. (2008) Detection of amino acetonitrile in Sgr B2(N). *Astron Astrophys* 482:179–196.

Belloche, A., Müller, H., Menten, K., Schilke, P., and Comito, C. (2013) Complex organic molecules in the interstellar medium: IRAM 30 m line survey of Sagittarius B2(N) and (M). *Astron Astrophys* 559:A47.

Belloche, A., Garrod, R.T., Müller, H.S.P., Menten, K.M., Medvedev, I., Thomas, J., and Kisiel, Z. (2019) Re-exploring molecular complexity with ALMA (ReMoCA): interstellar detection of urea. *Astron Astrophys* 628:A10.

Bernstein, M., Dworkin, J., Sandford, S., Cooper, G., and Allamandola, L. (2002) Racemic amino acids from the ultraviolet photolysis of interstellar ice analogues. *Nature* 416: 401–403.

Bisschop, S., Jørgensen, J., Bourke, T., Bottinelli, S., and van Dishoeck, E. (2008) An interferometric study of the low-mass protostar IRAS 16293-2422: small scale organic chemistry. *Astron Astrophys* 488:959–968.

Biver, N., Bockelée-Morvan, D., Moreno, R., Crovisier, J., Colom, P., Lis, D., Sandqvist, A., Boissier, J., Despois, D., and Milam, S. (2015) Ethyl alcohol and sugar in comet C/2014 Q2 (Lovejoy). *Sci Adv* 1:e1500863.

Caux, E., Kahane, C., Castets, A., Coutens, A., Ceccarelli, C., Bacmann, A., Bisschop, S., Bottinelli, S., Comito, C., Helmich, F., Lefloch, B., Parise, B., Schilke, P., Tielens, A., van Dishoeck, E., Vastel, C., Wakelam, V., and Walters, A. (2011) TIMASSS: the IRAS 16293-2422 millimeter and submillimeter spectral survey. *Astron Astrophys* 532:A23.

Ceccarelli, C., Loinard, L., Castets, A., Tielens, A.G.G.M., and Caux, E. (2000) The hot core of the solar-type protostar IRAS 16293-2422: H_2CO emission. *Astron Astrophys* 357:L9.

Ceccarelli, C., Caselli, P., Bockelée-Morvan, D., Mousis, O., Pizzarello, S., Robert, F., and Semenov, D. (2014) Deuterium fractionation: the Ariadne's thread from the precollapse phase to meteorites and comets today. In *Protostars and Planets VI*, edited by H. Beuther, R.S. Klessen, C.P. Dullemond and T. Henning, University of Arizona Press, Tucson, pp. 859–882.

Cheung, A.C., Rank, D.M., Townes, C.H., Thornton, D.D., and Welch, W.J. (1969) Detection of water in interstellar regions by its microwave radiation. *Nature* 221:626–628.

Ciaravella, A., Jiménez-Escobar, A., Cecchi-Pestellini, C., Huang, C.-H., Sie, N.-E., Muñoz Caro, G.M., and Chen, Y.-J. (2019) Synthesis of complex organic molecules in soft X-ray irradiated ices. *Eprint arXiv:1905.07958*.

Cocinero, E.J., Lesarri, A., Ecija, P., Basterretxea, F.J., Grabow, J.-U., Fernandez, J., A., and Castaño, F. (2012), Ribose found in the gas phase. *Angew Chem Int Ed* 51:3119–3124.

Collings, M., Anderson, M., Chen, R., Dever, J., Viti, S., Williams, D., and McCoustra, M. (2004) A laboratory survey of the thermal desorption of astrophysically relevant molecules. *Mon Not R Astron Soc* 354:1133–1140.

Coutens, A., Viti, S., Rawlings, J.M.C., Beltrán, M.T., Holdship, J., Jiménez-Serra, I., Quénard, D., and Rivilla, V.M. (2018a) Chemical modelling of glycolaldehyde and ethylene glycol in star-forming regions. *Mon Not R Astron Soc* 475: 2016–2026.

Coutens, A., Willis, E., Garrod, R., Müller, H., Bourke, T., Calcutt, H., Drozdovskaya, M., Jørgensen, J., Ligterink, N., Persson, M., Stéphan, G., van der Wiel, M., van Dishoeck, E., and Wampfler, S. (2018b) First detection of cyanamide (NH2CN) towards solar-type protostars. *Astron Astrophys* 612:A107.

De Marcellus, P., Modica, P., Meinert, C., Nahon, L., Meierhenrich, U.J., and Le Sergeant d'Hendecourt, L. (2014) VUV irradiation of interstellar ice analogues: an abiotic source for organic matter in planetary systems. *Eur Planet Sci Congr* 9: EPSC2014-72.

Douglas, A.E. and Herzberg, G. (1941) Note on CH+ in Interstellar Space and in the Laboratory. *Astrophys J* 94:381.

Dulieu, F., Nguyen, T., Congiu, E., Baouche, S., and Taquet, V. (2019) Efficient formation route of the prebiotic molecule formamide on interstellar dust grains. *Mon Not R Astron Soc Lett* 484:L119–L123.

Dzib, S., Ortiz-León, G., Hernández-Gómez, A., Loinard, L., Mioduszewski, A., Claussen, M., Menten, K., Caux, E., and Sanna, A. (2018) A revised distance to IRAS 16293-2422 from VLBA astrometry of associated water masers. *Astron Astrophys* 614:A20.

Écija, P., Uriarte, I., Spada, L., Davis, B.G., Walther, C., Basterretxea, F.J., Lesarri, A., and Cocinero, E.J. (2016), Furanosic forms of sugars: conformational equilibrium of methyl β-D-ribofuranoside. *Chem Commun* 52:6241–6244.

Endres, C.P., Schlemmer S., Schilke P., Stutzki J., and Mueller H.S.P. (2016) The Cologne Database for Molecular Spectroscopy, CDMS, in the virtual atomic and molecular data centre, VAMDC. *J Mol Spectrosc* 327:95–104.

Faure, A., Remijan, A., Szalewicz, K., and Wiesenfeld, L. (2014) Weak maser emission of methyl formate toward Sagittarius Bs(N) in the green bank telescope PRIMOS survey. *Astrophys J* 783:72.

Faure, A., Lique, F., and Remijan, A. (2018) Collisional excitation and weak maser action of interstellar methanimine. *J Phys Chem Lett* 9:3199–3204.

Fedoseev, G., Chuang, K.-J., van Dishoeck, E.F., Ioppolo, S., and Linnartz, H. (2016) Simultaneous hydrogenation and UV-photolysis experiments of NO in CO-rich interstellar ice analogues; linking HNCO, OCN⁻, NH2CHO, and NH2OH. *Mon Not R Astron Soc* 460:4297–4309.

Garrod, R.T. (2013) A three-phase chemical model of hot cores: the formation of glycine. *Astrophys J* 765:60.

Ginsburg, A., Bally, J., Barnes, A., Bastian, N., Battersby, C., Beuther, H., Brogan, C., Contreras, Y., Corby, J., Darling, J., De Pree, C., Galván-Madrid, R., Garay, G., Henshaw, J., Hunter, T., Kruijssen, J., Longmore, S., Lu, X., Meng, F., Mills, E., Ott, J., Pineda, J., Sánchez-Monge, Á., Schilke, P., Schmiedeke, A., Walker, D., and Wilner, D. (2018) Distributed star formation throughout the galactic center cloud Sgr B2. *Astrophys J* 853:171.

Goesmann, F., Rosenbauer, H., Bredehoft, J., Cabane, M., Ehrenfreund, P., Gautier, T., Giri, C., Kruger, H., Le Roy, L., MacDermott, A., McKenna-Lawlor, S., Meierhenrich, U., Caro, G., Raulin, F., Roll, R., Steele, A., Steininger, H., Sternberg, R., Szopa, C., Thiemann, W., and Ulamec, S. (2015) Organic compounds on comet 67P/Churyumov–Gerasimenko revealed by COSAC mass spectrometry. *Science* 349:aab0689–aab0689.

Goto, M., Indriolo, N., Geballe, T.R., and Usuda, T. (2013) H₃⁺ Spectroscopy and the ionization rate of molecular hydrogen in the central few parsecs of the galaxy. *J Phys Chem A* 117: 9919–9930.

Guesten, R., Walmsley, C.M., Ungerechts, H., and Churchwell, E. (1985) Temperature determinations in molecular clouds of the galactic center. *Astron Astrophys* 142:381–387.

Harada, N., Riquelme, D., Viti, S., Jimenez-Serra, I., Requena-Torres, M., Menten, Martin, S., Aladro, R., Martin-Pintado, J., and Hochgürtel, S. (2015) Chemical features in the circumnuclear disk of the Galactic center. *Astron Astrophys* 584: A102.

Herbst, E. and van Dishoeck, E.F. (2009) Complex organic interstellar molecules. *Annu Rev Astron Astrophys* 47:427–480.

Hernández-Gómez, A., Sahnoun, E., Caux, E., Wiesenfeld, L., Loinard, L., Bottinelli, S., Hammami, K., and Menten, K. (2019) Modelling the abundance structure of isocyanic acid (HNCO) towards the low-mass solar type protostar IRAS 16293-2422. *Mon Not R Astron Soc* 483:2014–2030.

Hollis, J.M., Lovas, F.J., and Jewell, P.R. (2000) Interstellar glycolaldehyde: the first sugar. *Astrophys J* 540:L107–L110.

Hollis, J.M., Jewell, P., Lovas, F., Remijan, A., and Møllendal, H. (2004) Green bank telescope detection of new interstellar aldehydes: propenal and propanal. *Astrophys J* 610:L21–L24.

Hüettemeister, S., Wilson, T.L., Bania, T.M., and Martín-Pintado, J. (1993) Kinetic temperatures in Galactic Center molecular clouds. *Astron Astrophys* 280:255–267.

Jaber, A., Ceccarelli, C., Kahane, C., and Caux, E. (2014) The census of complex organic molecules in the solar-type protostar IRAS16293-2422. *Astrophys J* 791:29.

Jeanvoine, Y. and Spezia, R. (2019) The formation of urea in space. II. MP2 vs PM6 dynamics in determining bimolecular reaction products. *Theor Chem Acc* 138:1.

Jiménez-Serra, I., Testi, L., Caselli, P., and Viti, S. (2014) Detectability of glycine in solar-type system precursors. *Astrophys J Lett* 787:L33–L38.

Jiménez-Serra, I., Vasyunin, A., Caselli, P., Marcelino, N., Billot, N., Viti, S., Testi, L., Vastel, C., Lefloch, B., and Bachiller, R. (2016) The spatial distribution of complex organic molecules in the L1544 pre-stellar core. *Astrophys J* 830:L6.

Jørgensen, J., van der Wiel, M., Coutens, A., Lykke, J., Müller, H., van Dishoeck, E., Calcutt, H., Bjerkeli, P., Bourke, T., Drozdovskaya, M., Favre, C., Fayolle, E., Garrod, R., Jacobsen, S., Öberg, K., Persson, M., and Wampfler, S. (2016) The ALMA protostellar interferometric line survey (PILS)—first results from an unbiased submillimeter wavelength line survey of the Class 0 protostellar binary IRAS 16293-2422 with ALMA. *Astron Astrophys* 595:A117.

Kitadai, N. and Maruyama, S. (2018) Origins of building blocks of life: a review. *Geosci Front* 9:1117–1153.

Krieger, N., Ott, J., Beuther, H., Walter, F., Kruijssen, J., Meier, D., Mills, E., Contreras, Y., Edwards, P., Ginsburg, A., Henkel, C., Henshaw, J., Jackson, J., Kauffmann, J., Longmore, S., Martín, S., Morris, M., Pillai, T., Rickert, M., Rosolowsky, E., Shinnaga, H., Walsh, A., Yusef-Zadeh, F., and Zhang, Q. (2017) The survey of water and ammonia in the galactic center (SWAG): molecular cloud evolution in the central molecular zone. *Astrophys J* 850:77.

Kuan, Y., Yan, C., Charnley, S., Kisiel, Z., Ehrenfreund, P., and Huang, H. (2003) A search for interstellar pyrimidine. *Mon Not R Astron Soc* 345:650–656.

Laas, J.C., Garrod, R.T., Herbst, E., and Widicus Weaver, S.L. (2011) Contributions from grain surface and gas phase chemistry to the formation of methyl formate and its structural isomers. *Astrophys J* 728:71–80.

Larralde, R., Robertson, M., and Miller, S. (1995) Rates of decomposition of ribose and other sugars: implications for chemical evolution. *Proc Natl Acad Sci USA* 92:8158–8160.

Ligterink, N.F.W., Terwisscha van Scheltinga, J., Taquet, V., Jørgensen, J.K., Cazaux, S., van Dishoeck, E.F., and Linnartz, H. (2018) The formation of peptide-like molecules on interstellar dust grains. *Mon Not R Astron Soc* 480:3628–3643.

Lykke, J., Coutens, A., Jørgensen, J., van der Wiel, M., Garrod, R., Müller, H., Bjerkeli, P., Bourke, T., Calcutt, H., Drozdovskaya, M., Favre, C., Fayolle, E., Jacobsen, S., Öberg, K., Persson, M., van Dishoeck, E., and Wampfler, S. (2016) The ALMA-PILS survey: first detections of ethylene oxide, acetone and propanal toward the low-mass protostar IRAS 16293-2422. *Astron Astrophys* 597:A53.

Martín, S., Requena-Torres, M., Martín-Pintado, J., and Mauersberger, R. (2008) Tracing shocks and photodissociation in the galactic center region1. *Astrophys J* 678:245–254.

Martín-Doménech, R., Rivilla, V., Jiménez-Serra, I., Quénard, D., Testi, L., and Martín-Pintado, J. (2017) Detection of methyl isocyanate (CH3NCO) in a solar-type protostar. *Mon Not R Astron Soc* 469:2230–2234.

McCaffrey, V.P., Zellner, N.E.B., Waun, C.M., Bennett, E.R., and Earl, E.K. (2014) Reactivity and survivability of glycolaldehyde in simulated meteorite impact experiments. *Origins Life Evol B* 44:29–42.

McGuire, B.A. (2018) 2018 Census of interstellar, circumstellar, extragalactic, protoplanetary disk, and exoplanetary molecules. *Astrophys J Suplement Series* 239:17–65.

McMullin, J.P., Waters, B., Schiebel, D., Young, W., and Golap, K. (2007) *Astronomical Data Analysis Software and Systems XVI* (ASP Conf. Ser. 376), ed. R.A. Shaw, F. Hill and D.J. Bell, ASP, San Francisco, CA, p. 127.

Meinert, C., Myrgorodska, I., de Marcellus, P., Buhse, T., Nahon, L., Hoffmann, S., d'Hendecourt, L., and Meierhenrich, U. (2016) Ribose and related sugars from ultraviolet irradiation of interstellar ice analogs. *Science* 352:208–212.

Miller, S.L. (1953) Production of amino acids under possible primitive earth conditions. *Science* 117:528–529.

Møllendal, H. and Konovalov, A. (2010) Microwave spectrum of 2-aminooxazole, a compound of potential prebiotic and astrochemical interest. *J Phys Chem A* 114:2151–2156.

Morris, M. and Serabyn, E. (1996) The Galactic Center Environment. *Annu Rev Astron Astrophys* 34:645–702.

Muñoz Caro, G.M., Meierhenrich, U., Schutte, W., Barbier, B., Arcones Segovia, A., Rosenbauer, H., Thiemann, W., Brack, A., and Greenberg, J. (2002) Amino acids from ultraviolet irradiation of interstellar ice analogues. *Nature* 416:403–406.

Muñoz Caro, G.M., Dartois, E., Boduch, P., Rothard, H., Domaracka, A., and Jiménez-Escobar, A. (2014) Comparison of UV and high-energy ion irradiation of methanol:ammonia ice. *Astron Astrophys* 566:93–101.

Oró, J. and Kimball A.P. (1961) Synthesis of purines under possible primitive earth conditions. I. Adenine from hydrogen cyanide. *Arch Biochem Biophys* 94:217–227.

Patel, B.H., Percivalle, C., Ritson, D.J., Duffy, C.D., and Sutherland, J.D. (2015) Common origins of RNA, protein and lipid precursors in a cyanosulfidic protometabolism. *Nat Chem* 7:301–307.

Peña, I., Cocinero, E.J., Cabezas, C., Lesarri, A., Mata, S., Écija, P., Daly, A.M., Cimas, A., Bermúdez, C., Basterretxea, F.J., Blanco, S., Fernández, J.A., López, J.C., Castaño, F., and Alonso, J.L. (2013) Six pyranoside forms of free 2-deoxy-D-ribose. *Angew Chem Int Ed* 52:11840–11845.

Persson, M., Jørgensen, J., Müller, H., Coutens, A., van Dishoeck, E., Taquet, V., Calcutt, H., van der Wiel, M., Bourke, T., and Wampfler, S. (2018) The ALMA-PILS survey: formaldehyde deuteration in warm gas on small scales toward IRAS 16293-2422 B. *Astron Astrophys* 610:A54.

Pickett, H.M. (1991) The fitting and prediction of vibration-rotation spectra with spin interactions, *J Mol Spectrosc* 148:371–377.

Pickett, H.M., Poynter, R.L., Cohen, E.A., Delitsky, M.L., Pearson, J.C., and Muller, H.S.P. (1998) Submillimeter, millimeter and microwave spectral line catalog. *J Quant Spectrosc Radiat Transf* 60:883–890.

Pineda, J., Maury, A., Fuller, G., Testi, L., García-Appadoo, D., Peck, A., Villard, E., Corder, S., van Kempen, T., Turner, J., Tachihara, K., and Dent, W. (2012) The first ALMA view of IRAS 16293-2422. Direct detection of infall onto source B and high-resolution kinematics of source A. *Astron Astrophys* 544:L7.

Powner, M.W., Gerland, B., and Sutherland, J.D. (2009) Synthesis of activated pyrimidine ribonucleotides in prebiotically plausible conditions. *Nature* 459:239–242.

Quénard, D., Jiménez-Serra, I., Viti, S., Holdship, J., and Coutens, A. (2018) Chemical modelling of complex organic molecules with peptide-like bonds in star-forming regions. *Mon Not R Astron Soc* 474:2796–2812.

Reid, M., Menten, K., Brunthaler, A., Zheng, X., Dame, T., Xu, Y., Wu, Y., Zhang, B., Sanna, A., Sato, M., Hachisuka, K., Choi, Y., Immer, K., Moscadelli, L., Rygl, K., and Bartkiewicz, A. (2014) Trigonometric parallaxes of high mass star forming regions: the structure and kinematics of the milky way. *Astrophys J* 783:130.

Requena-Torres, M., Martín-Pintado, J., Rodríguez-Franco, A., Martín, S., Rodríguez-Fernández, N., and de Vicente, P. (2006) Organic molecules in the Galactic center. *Astron Astrophys* 455:971–985.

Requena-Torres, M., Martín-Pintado, J., Martín, S., and Morris, M. (2008) The galactic center: the largest oxygen-bearing organic molecule repository. *Astrophys J* 672:352–360.

Rivilla, V.M., Fontani, F., Beltrán, M., Vasyunin, A., Caselli, P., Martín-Pintado, J., and Cesaroni, R. (2016) The first detections of the key prebiotic molecule PO in star-forming regions. *Astrophys J* 826:161.

Rivilla, V.M., Beltran, M.T., Cesaroni, R., Fontani, F., Codella, C., and Zhang, Q. (2017) Formation of ethylene glycol and other complex organic molecules in star-forming regions. *Astron Astrophys* 598A:59–82.

Rivilla, V.M., Jiménez-Serra, I., Zeng, S., Martín, S., Martín-Pintado, J., Armijos-Abendaño, J., Viti, S., Aladro, R., Riquelme, D., Requena-Torres, M., Quénard, D., Fontani, F., and Beltrán, M. (2018) Phosphorus-bearing molecules in the Galactic Center. *Mon Not R Astron Soc Lett* 475:L30–L34.

Rivilla, V.M., Beltrán, M.T., Vasyunin, A., Caselli, P., Viti, S., Fontani, F., and Cesaroni, R. (2019a) First ALMA maps of HCO, an important precursor of complex organic molecules, towards IRAS 16293-2422. *Mon Not R Astron Soc* 483:806–823.

Rivilla, V.M., Martín-Pintado, J., Jiménez-Serra, I., Zeng, S., Martín, S., Armijos-Abendaño, J., Requena-Torres, M.A., Aladro, R., and Riquelme, D. (2019b) Abundant Z-cyanomethanimine in the interstellar medium: paving the way to the synthesis of adenine. *Mon Not R Astron Soc* 483:L114–L119.

Rodríguez-Fernández, N.J., Martín-Pintado, J., de Vicente, P., Fuente, A., Hüttemeister, S., Wilson, T.L., and Kunze, D. (2000) Non-equilibrium H_2 ortho-to-para ratio in two molecular clouds of the Galactic Center. *Astron Astrophys* 356:695–704.

Rodríguez-Fernández, N.J., Martín-Pintado, J., Fuente, A., and Wilson, T.L. (2004) ISO observations of the galactic center interstellar medium. Neutral gas and dust. *Astron Astrophys* 427:217–229.

Ruiz-Mirazo, K., Briones, C., and de la Escosura, A. (2014) Prebiotic systems chemistry: new perspectives for the origins of life. *Chem Rev* 114:285–366.

Skouteris, D., Vazart, F., Ceccarelli, C., Balucani, N., Puzzarini, C., and Barone, V. (2017) New quantum chemical compu-

tations of formamide deuteration support gas-phase formation of this prebiotic molecule. *Mon Not R Astron Soc Lett* 468: L1–L5.

Skouteris, D., Balucani, N., Ceccarelli, C., Vazart, F., Puzzarini, C., Barone, V., Codella, C., and Lefloch, B. (2018) The genealogical tree of ethanol: gas-phase formation of glycolaldehyde, acetic acid, and formic acid. *Astrophys J* 854:135–145.

Snyder, L.E. and Buhl, D. (1971) Observations of radio emission from interstellar hydrogen cyanide. *Astrophys J* 163: L47–L52.

Suzuki, T., Majumdar, L., Ohishi, M., Saito, M., Hirota, T., and Wakelam, V. (2018) An expanded gas-grain model for interstellar glycine. *Astrophys J* 863:51–69.

Swings, P. and Rosenfeld, L. (1937) Considerations regarding interstellar molecules. *Astrophys J* 86:483–486.

Takakuwa, S., Ohashi, N., Bourke, T.L., Hirano, N., Ho, P.T.P., Jørgensen, J.K., Kuan, Y.-J., Wilner, D.J., and Yeh, S.C.C. (2007) Arcsecond-resolution submillimeter HCN imaging of the binary protostar IRAS 16293-2422. *Astrophys J* 662:431–442.

Turner, B.E., Liszt, H.S., Kaifu, N., and Kisliakov, A.G. (1975) Microwave detection of interstellar cyanamide. *Astrophys J* 201:L149–L152.

Wampfler, S., Jørgensen, J., Bizzarro, M., and Bisschop, S. (2014) Observations of nitrogen isotope fractionation in deeply embedded protostars. *Astron Astrophys* 572:A24.

Whittet, D. and Duley, W. (1991) Carbon monoxide frosts in the interstellar medium. *Astron Astrophys Rev* 2:167–189.

Widicus Weaver, S. and Blake, G. (2005) 1,3-Dihydroxyacetone in Sagittarius B2(N-LMH): The First Interstellar Ketose. *Astrophys J* 624:L33–L36.

Wilson, T. and Rood, R. (1994) Abundances in the interstellar medium. *Annu Rev Astron Astrophys* 32:191–226.

Woods, P.M., Slater, B., Raza, Z., Viti, S., Brown, W.A., and Burke, D.J. (2013) Glycolaldehyde formation via the dimerization of the formyl radical. *Astrophys J* 777:90.

Zapata, L., Loinard, L., Rodríguez, L., Hernández-Hernández, V., Takahashi, S., Trejo, A., and Parise, B. (2013) ALMA 690 GHz observations of IRAS 16293-2422B: infall in a highly optically thick disk. *Astrophys J* 764:L14.

Zeng, S., Jiménez-Serra, I., Rivilla, V., Martín, S., Martín-Pintado, J., Requena-Torres, M., Armijos-Abendaño, J., Riquelme, D., and Aladro, R. (2018) Complex organic molecules in the Galactic Centre: the N-bearing family. *Mon Not R Astron Soc* 478:2962–2975.

Zeng, S., Quénard, D., Jiménez-Serra, I., Martín-Pintado, J., Rivilla, V.M., Testi, L., and Martín-Doménech, R. (2019) First detection of the pre-biotic molecule glycolonitrile ($HOCH_2CN$) in the interstellar medium. *Mon Not R Astron Soc* 484:L43–L48.

Address correspondence to:
Izaskun Jiménez-Serra
Departamento de Astrofísica
Centro de Astrobiología (CSIC-INTA)
Carretera de Torrejon a Ajalvir km 4
Torrejón de Ardoz, Madrid 28850
Spain

E-mail: ijimenez@cab.inta-csic.es

Abbreviations Used

Δv = linewidth
ALMA = Atacama Large Millimeter/
Submillimeter Array
$C_3H_4N_2O$ = 2-amino-oxazole
CDMS = Cologne Database for Molecular
Spectroscopy
$CH_2(OH)CHO$ = glycolaldehyde
CH_2NH = methanimine
$CH_2OHCOOH$ = glycolic acid
CH_3NCO = methyl isocyanate
$CHOCHOHCH_2OH$ = glyceraldehyde
COMs = complex organic molecules
CSM = circumstellar medium
DHA = dihydroxyacetone; $CH_2OHCOCH_2OH$
E/Z-HNCHCN = E-/Z-cyanomethanimine
E_l = lower level
EMIRs = Eight MIxer Receivers
GMC = giant molecular cloud
H_2CO = formaldehyde

$HC^{15}N$ = ^{15}N isotopologue of HCN
HCN = hydrogen cyanide
HNCHCN = cyanomethanimine
$HOCH_2CN$ = glycolonitrile
IRAM = Instituto de Radioastronomía
Milimétrica
ISM = interstellar medium
JPL = Jet Propulsion Laboratory
LTE = local thermodynamical
equilibrium
MADCUBA = Madrid Data Cube Analysis
NH_2CH_2CN = aminoacetonitrile
NH_2CH_2COOH = glycine
NH_2CHO = formamide
NH_2CN = cyanamide
NH_2CONH_2 = urea
N_{tot} = molecular column density
T_{ex} = excitation temperature
UV = ultraviolet
V_{LSR} = central radial velocity